1-2019

Dorsal Raphe Dual Serotonin-Glutamate Neurons Drive Reward by Establishing Excitatory Synapses on VTA Mesoaccumbens Dopamine Neurons

H-L. Wang

S. Zhang

J. Qi

H. Wang

R. Cachope

See next page for additional authors

Repository Citation

Wang, H-L., Zhang, S., Qi, J., Wang, H., Cachope, R., Mejias-Aponte, C. A., Gomez, J. A., ... & Morales, M. (2019). Dorsal raphe dual serotonin-glutamate neurons drive reward by establishing excitatory synapses on VTA mesoaccumbens dopamine neurons. *Cell Reports, 26*(5), 1128-1142.e7. https://doi.org/10.1016/j.celrep.2019.01.014

Published in final edited form as:

Cell Rep. 2019 January 29; 26(5): 1128–1142.e7. doi:10.1016/j.celrep.2019.01.014.

Dorsal Raphe Dual Serotonin-Glutamate Neurons Drive Reward by Establishing Excitatory Synapses on VTA Mesoaccumbens Dopamine Neurons

Hui-Ling Wang[1,5], **Shiliang Zhang**[2,5], **Jia Qi**[1,5], **Huikun Wang**[1], **Roger Cachope**[3], **Carlos A. Mejias-Aponte**[1], **Jorge A. Gomez**[4], **Gabriel E. Mateo-Semidey**[1], **Gerard M.J. Beaudoin**[4], **Carlos A. Paladini**[4], **Joseph F. Cheer**[3], and **Marisela Morales**[1,6,*]

[1]National Institute on Drug Abuse, Neuronal Networks Section, NIH, Baltimore, MD, USA

[2]National Institute on Drug Abuse, Electron Microscopy Core, NIH, Baltimore, MD, USA

[3]Department of Anatomy and Neurobiology, University of Maryland School of Medicine, Baltimore, MD, USA

[4]Department of Biology, University of Texas at San Antonio, San Antonio, TX, USA

[5]These authors contributed equally

[6]Lead Contact

SUMMARY

Dorsal raphe (DR) serotonin neurons provide a major input to the ventral tegmental area (VTA). Here, we show that DR serotonin transporter (SERT) neurons establish both asymmetric and symmetric synapses on VTA dopamine neurons, but most of these synapses are asymmetric. Moreover, the DR-SERT terminals making asymmetric synapses on VTA dopamine neurons coexpress vesicular glutamate transporter 3 (VGluT3; transporter for accumulation of glutamate for its synaptic release), suggesting the excitatory nature of these synapses. VTA photoactivation of DR-SERT fibers promotes conditioned place preference, elicits excitatory currents on mesoaccumbens dopamine neurons, increases their firing, and evokes dopamine release in nucleus accumbens. These effects are blocked by VTA inactivation of glutamate and serotonin receptors, supporting the idea of glutamate release in VTA from dual DR SERT-VGluT3 inputs. Our findings suggest a path-specific input from DR serotonergic neurons to VTA that promotes reward by the release of glutamate and activation of mesoaccumbens dopamine neurons.

*Correspondence: mmorales@intra.nida.nih.gov.

AUTHOR CONTRIBUTIONS

M.M., H.-L.W., S.Z., and J.Q. designed the experiments. H-L.W., S.Z., J.Q., H.W., R.C., C.A.M.A., J.A.G., G.E.M.S., and G.M.J.B. performed the experiments. H.-L.W., S.Z., J.Q., H.W., C.A.M.A., J.A.G., G.E.M.S., G.M.J.B., and M.M. analyzed the data. M.M. wrote the paper with the contribution of all co-authors.

DECLARATION OF INTERESTS

The authors declare no competing interests.

SUPPLEMENTAL INFORMATION

Supplemental Information includes seven figures and two tables and can be found with this article online at https://doi.org/10.1016/j.celrep.2019.01.014.

INTRODUCTION

Although selective serotonin uptake inhibitors comprise the major class of modern antidepressants, the role of serotonin in reward function remains poorly understood. Lesion and pharmacological studies implicate serotonin in a wide array of cognitive and behavioral functions, including mood and reward (Lucki, 1998). Alterations in serotonergic function and reward-related processing have been hypothesized in several psychiatric disorders, including schizophrenia (Kapur and Remington, 1996; Ziauddeen and Murray, 2010), depression (McCabe et al., 2012; Nestler and Carlezon, 2006; Ruf and Bhagwagar, 2009; Watson and Dawson, 2007), and drug abuse (Higgins and Fletcher, 2003; Kirby et al., 2011; Müller et al., 2007; Vengeliene et al., 2008).

The role of serotonin in reward-related processing has been investigated for several decades, and although some have previously suggested that serotonin is antagonistic to reward function, the literature describing the role of serotonin in reward is equivocal (Boureau and Dayan, 2011; Cools et al., 2011; Hayes and Greenshaw, 2011; Kranz et al., 2010). The inhibitory role of serotonin in reward function was initially suggested from studies showing that depletion of serotonin increased responding for brain-stimulation reward (Phillips etal., 1976; Poschel and Ninteman, 1971; Poschel et al., 1974) and from studies in which local inhibition of serotonin neurons facilitated brain stimulation reward (Fletcher et al., 1995) or established conditioned place preference (Fletcher et al., 1993). Place preference was also observed after pharmacological manipulations aimed to inhibit serotonergic function (Liu and Ikemoto, 2007; Shin and Ikemoto, 2010). In contrast, direct electrical stimulation of the dorsal raphe (DR) is rewarding (Deakin, 1980; Miliaressis et al., 1975; Rompre and Miliaressis, 1985; Simon et al., 1976; Van Der Kooy et al., 1978), and DR *in vivo* recordings in monkeys (Bromberg-Martin et al., 2010; Nakamura et al., 2008) and rats (Miyazaki et al., 2011; Ranade and Mainen, 2009) suggest that DR neurons are activated by reward and contribute to reward function.

Recent recordings from genetically identified serotonin neurons have provided evidence for neuronal activation of some DR serotonin neurons in response to cues predicting reward (Cohen et al., 2015; Liu et al., 2014) or reward consumption (Li et al., 2016). In addition, behavioral studies have shown that photoactivation of DR serotonin neurons reinforces instrumental behavior (Li et al., 2016; Liu et al., 2014). However, other studies have reported that photoactivation of DR serotonin neurons do not reinforce behavior (Fonseca et al., 2015; McDevitt et al., 2014). Because global serotonin brain manipulations can alter multiple serotonergic projections and transduction pathways as well as multiple components of a given aspect of reinforcement, the role of serotonin on reward function may be better understood by studying the contribution of specific serotonergic pathways. In this regard, DR serotonin neurons heavily innervate the ventral tegmental area (VTA) (Bobillier et al., 1976; Pierce et al., 1976), the origin of the mesolimbic dopamine system, a network of known importance for reward and motivational function (Wise, 2004). Immuno ultrastructural studies have demonstrated that DR serotonin neurons establish synaptic contacts on VTA dopamine neurons (Hervé et al., 1987; Van Bockstaele et al., 1994), and pharmacological and electrophysiological studies have shown that serotonin is capable of inhibiting or exciting VTA dopamine neurons. The mixed effects of serotonin on VTA

dopamine neurons is likely to reflect activation of multiple serotonin receptor subtypes, some of which excite or inhibit dopamine neurons (Alex and Pehek, 2007; Cameron et al., 1997; Di Giovanni et al., 2008; Pessia et al., 1994). Nevertheless, a role of VTA in serotonin-mediated reward was initially proposed from studies showing that infusion of serotonin into the VTA potentiates medial forebrain bundle electrical self-stimulation (Redgrave and Horrell, 1976).

In the present study, we examined the ultrastructural and molecular characteristics of the synaptic connectivity between DR serotonin neurons and VTA dopamine neurons and determined the role of these connections in behavior. Our results demonstrate that axon terminals from DR serotonin neurons establish symmetric or asymmetric synapses on VTA dopamine neurons. We found that the axon terminals from DR serotonin neurons making asymmetric (putative excitatory) synapses on VTA dopamine neurons coexpress vesicular glutamate transporter 3 (VGluT3). VTA activation of DR serotonin terminals elicits excitation of dopamine neurons, and the release of serotonin and glutamate from these terminals activates serotonin and glutamate receptors, induces release of dopamine in nucleus accumbens (nAcc), and promotes conditioned place preference (CPP).

RESULTS

SERT and Dual SERT-VGluT3 Axon Terminals Differentially Synapse on VTA Dopamine Neurons

Tracing studies in the rat have shown that two types of DR serotonergic neurons innervate the VTA; serotonin-only and dual serotonin-VGluT3 neurons (Geisler et al., 2007; Hioki et al., 2010). Here, we examined, in mouse VTA, the frequency of axon terminals (punctate structures containing synaptophysin) expressing SERT alone (SERT-only terminals) or together with VGluT3 (SERT-VGluT3 terminals) (Figure 1A). We determined that, from a population of 14,342 counted SERT terminals in the VTA, 67.66% ± 1.43% were SERT-only and 32.34% ± 1.43% were dual SERT-VGluT3 terminals (Figure 1B; $t_{(3)} = 12.33$, $p = 0.0011$).

By triple-immunolabeling and electron microscopy, we determined the extent to which SERT-only or SERT-VGluT3 terminals synapse on VTA dopamine neurons (expressing tyrosine hydroxylase [TH]). Given that VGluT3 and SERT are each confined to presynaptic compartments in VTA and TH has a postsynaptic distribution in dendrites and cell bodies (Bayer and Pickel, 1991; Carr and Sesack, 2000; Omelchenko and Sesack, 2005), this segregation allowed us the simultaneous detection of presynaptic VGluT3 or SERT and postsynaptic TH. By electron microscopy, we found that terminals from both SERT-only and SERT-VGluT3 neurons established synapses on VTA TH-neurons, but 61.17% ± 2.59% were from SERT-VGluT3 terminals ($t_{(3)} = 4.313$, $p = 0.0230$; 150 of 251 SERT-VGluT3 terminals) and 36.99% ± 3.72% from SERT-only terminals (36.99% ± 3.72%, $t_{(3)} = 3.498$, $p = 0.0395$; 180 of 535 SERT-only terminals) (Figures 1C, 1D, and S1). Furthermore, we found that SERT-positive terminals establishing *asymmetric* synapses on VTA TH-positive neurons coexpressed VGluT3, suggesting that serotonergic terminals establishing asymmetric synapses are excitatory because of their capability to co-release glutamate. These findings indicate that, within the VTA, TH-positive neurons are the major target of

dual SERT-VGluT3 neurons and that most DR serotonin neurons synapsing on TH-positive neurons are from dual SERT-VGluT3 neurons.

We next determined whether DR-SERT-VGluT3 neurons synapse on TH neurons that innervate nAcc (mesoaccumbens neurons). For these studies, we injected an adeno-associated virus (AAV, encoding Cre-dependent channelrhodopsin-2 [ChR2], tethered to mCherry or enhanced yellow fluorescent protein [eYFP]) in DR of SERT::Cre mice (referred to here as SERT-ChR2-mCherry or SERT-ChR2-eYFP mice) to drive expression of ChR2-mCherryorChR2-eYFPin DR-SERT neurons (Figure 2). Next, in the nAcc of these mice, we injected the retrograde tract tracer Fluoro-Gold (FG) to tag mesoaccumbens neurons (Figures 2A, 2A', and S2A). We observed that DR inputs mostly innervated the lateral VTA, where most FG-positive neurons were detected, FG-neurons that were mostly TH-positive (81.02%; 397 of 490 FG neurons). Then, by quadruple immunofluorescence, we found that SERT-VGluT3 axon terminals targeted dual FG-TH dendrites, which were confined to lateral VTA (Figures 2B–2D). By VTA electron microscopy, we confirmed that dual SERT-VGluT3 axon terminals made asymmetric synapses on dendrites coexpressing TH and FG (Figures 2E–2G). Together these fluorescence and ultrastructural findings indicate that dopamine mesoaccumbens neurons are a major target of dual DR serotonergic-VGluT3 neurons. These anatomical findings provide evidence suggesting an excitatory control of mesoaccumbens VTA dopamine neurons by dual SERT-VGluT3 afferents from DR neurons.

VTA Optical Activation of SERT Fibers Evokes Excitatory Currents on Mesoaccumbens Dopamine Neurons

Published studies using whole-cell patch-clamp recordings have shown that optical stimulation of inputs from *Pet-1* neurons (express mostly in serotonergic neurons) releases glutamate and serotonin within the VTA (Liu et al., 2014). To directly test glutamate release from serotonergic neurons on VTA dopamine neurons innervating nAcc, we prepared VTA slices from SERT-ChR2-eYFP mice that were also injected in nAcc with the retrograde tracer cholera toxin subunit B (CTb) (n =6 mice; Figures 2H and S2B). We performed patch-clamp recordings from 24 CTb-labeled (mesoaccumbens) neurons distributed in the lateral VTA and found that VTA optical stimulation of SERT-fibers evoked excitatory postsynaptic currents (EPSCs) in seven of the CTb recorded neurons, whose currents were abolished by α-amino-3-hydroxy-5-methyl-4-isoxazolepropionic acid (AMPA) receptor antagonist 6-cyano-7-nitroquinoxaline-2,3-dione (CNQX) (Figure 2J). We filled the recorded neurons with biocytin and found that five CTb-recorded neurons showing optical-evoked EPSCs were TH positive (Figure 2I). To determine whether DR-SERT inputs are capable of exciting TH mesoaccumbens neurons, we performed VTA cell-attached and current-clamp recordings in response to optical stimulation and found increased firing of three CTb-TH neurons (Figure 2K). The optical-evoked EPSCs were eliminated by bath application of tetrodotoxin (TTX; 500 nM) and were restored by application of 4-aminopyridine (4-AP; 200 μM) (Figure S3), suggesting that optical-evoked EPSCs are mediated by monosynaptic glutamatergic transmission. These findings indicate that VTA glutamate release from DR dual SERT-VGluT3 terminals is capable of evoking the firing of mesoaccumbens dopamine neurons.

In addition, by whole-cell voltage-clamp recordings, we found that either 0.5-ms pulses of VTA electrical stimulation of DR fibers or 2-ms pulses of VTA optical stimulation of DR-SERT fibers evoked EPSCs on VTA dopamine neurons, clamped at −60 mV and found that those currents decreased after VTA blockade of 5-HT_3 receptor antagonist Y-25130. As a result of 5-TH_3 receptor blockade, the current evoked by optical stimulation decreased from 63.78 ± 20.8 pA to 53.07 ± 19.22 pA (Figures 3A and 3B), and that evoked by electrical stimulation decreased from −1,686 ± 322.7 pA to −1,511 ± 262.6 pA (Figures 3D and 3E). The 5-HT_3 receptor-mediated current was calculated by subtracting the total current from the current remaining after 5-HT_3 receptor antagonism (optical 5-HT_3-mediated current = 13.14 ± 3.3 pA; electrical 5-HT_3-mediated current = 80.3 ± 46.33 pA). Additionally, the rise time of the optically evoked, 5-HT_3-mediated current was faster (0.47 ± 0.094 ms) than the remaining current (0.84 ± 0.11 ms; Figure 3C). This kinetic characteristic was also similar for electrical stimulation, faster (0.60 ± 0.094 ms) than the remaining current (0.79 ± 0.23 ms), although that was not statistically significant (paired t test, $p > 0.05$, $n = 3$). We found that blockade of 5-HT_3 receptors increased the optically induced, paired pulse ratio (from 0.34 ± 0.1 to 0.62 ± 0.12; Figure 3F), suggesting that 5-HT_3 receptors can also affect the probability of neurotransmitter release. These findings indicate that VTA release of serotonin from DR inputs excites dopamine neurons via activation of 5-HT_3 receptors.

By *in vivo* VTA recordings in urethane-anesthetized mice, we found that VTA optical stimulation of SERT fibers evoked either neuronal excitation or inhibition (Figure 3G). From a total of 80 VTA-recorded neurons in response to photoactivation of the DR to VTA pathway, 20% (16 of 80) of the neurons were excited and 28.8% (23 of 80) were inhibited (Figure 3H); the excitatory and the inhibitory responses had similar onset (reaching significance at 1.5 s after stimulus) and duration (6.5 s from prestimulation firing rates to onset; Figures 3I and 3J). Among the neurons that showed excitation, 50% (8 of 16) remained excited during the 6 s immediately after the stimulus, and in only one of those neurons was the excitation followed by inhibition (Figure 3I, individual traces). Among the neurons that were inhibited, 44% (10 of 23) remained inhibited during the 6 s immediately after the stimulus, and in 21.8% (5 of 23) of those neurons, the inhibition was followed by excitation (Figure 3J, individual traces).

These findings from *in vitro* and *in vivo* VTA recordings, together with those from immuno ultrastructural studies (Figures 1C and 1D), indicate that (1) some SERT inputs from DR to VTA release glutamate, and (2) DR dual SERT-VGluT3 terminals establish asymmetric synapses, mostly on TH neurons, and have an excitatory effect on some dopamine neurons that innervate the nAcc.

DR-SERT Inputs Targeting VTA Promote nAcc Dopamine Release

We next determined whether stimulation of DR neurons or their VTA inputs produce release of dopamine in nAcc. We first tested the effects of DR electrical stimulation on nAcc dopamine release (Figures S4A–S4D) because previous studies had reported that electrical stimulation of DR inhibits dopamine neurons (Dray et al., 1976; Trent and Tepper, 1991; Tsai, 1989). In contrast with previous, published findings, we found that DR electrical stimulation evoked rapid and robust release of dopamine in nAcc core, as measured by fast-

scan cyclic voltammetry (Figure S4). We administered the D_2-receptor antagonist eticlopride (2 mg/kg, intraperitoneally [i.p.]) to confirm that the principal electrochemical contribution to the signal was from dopamine. Eticlopride treatment significantly increased the signal due to autoreceptor blockade (Figures S4B and S4C), suggesting that the recorded electrochemical analyte was dopamine. Additionally, we did not detect changes in the rate of decay of the signal in the nAcc of animals that received systemic administration of the serotonin reuptake inhibitor fluoxetine (10 mg/kg, i.p.), suggesting that serotonin was not released in a detectable fashion in the nAcc core after DR stimulation (Figure S4D). Because previous *in vivo* microdialysis studies have shown that 5-HT3 receptors affect dopamine release within the mesoaccumbens system (Campbell et al., 1996; Imperato and Angelucci, 1989; McBride et al., 2004), we tested the effect of ondansetron on evoked accumbal dopamine release driven by DR electrical stimulation. We found that the baseline (predrug) level of dopamine release in nAcc core evoked by DR electrical stimulation (Figures S4E–S4G; 141.9 ± 8.8 nM, n = 4) was significantly reduced by systemic application of ondansetron (2 mg/kg i.p.) (Figure S4E; 89.4 ± 5.0 nM, $p < 0.01$, n = 4). Importantly, we recapitulated the findings obtained after systemic pharmacology by demonstrating a significant reduction of dopamine release following intra-VTA microinjections (3 μg/0.3 μL) (Figures S5A and S5B) of either ondansetron (42.3% ± 2.9%) or CNQX (47.3% ± 1.9%; Figures S4H and S4I). Together, these results suggest that DR excitatory effects on VTA through 5-HT3 and glutamatergic receptors drive mesoaccumbens release of dopamine. We next measured nAcc dopamine release in the nAcc core, as evoked by VTA optical stimulation of DR-SERT inputs (Figures 4A–4D, S5C, and S5D‘). Dopamine release in the nAcc core evoked by optical stimulation of DR-SERT neurons (54.8 ± 2.9 nM) or SERT fibers in VTA (38.9 ± 5.9 nM) was significantly increased after systemic application of eticlopride (2 mg/kg i.p.) (Figure 4D; 99.6 ± 9.8 nM for stimulation of DR, 115.3 ± 11.8 nM for stimulation of VTA SERT fibers).

In a follow-up study, we evaluated dopamine release in nAcc of freely moving mice by microdialysis coupled to electrochemical detection (Figures 4E and 4F). We found that basal, extracellular nAcc dopamine levels were not significantly different between SERT-eYFP control mice (0.39 ± 0.01 nM, n = 6) and SERT-ChR2-eYFP mice (0.38 ± 0.02 nM, n = 18). Consistent with results from the fast-scan cyclic voltammetry, we found that VTA optical stimulation of SERT fibers significantly increased dopamine concentrations in nAcc (Figure 4F). To determine whether 5-HT_3 receptors or glutamate receptors on VTA dopamine neurons mediated that effect, we injected 0.2 μL of ondansetron (3 μg) in the VTA of SERT-ChR2-eYFP mice or 1 μg of CNQX 10 min before photostimulation. Dopamine release induced by VTA photostimulation of SERT fibers was blocked by both ondansetron and CNQX, but was unaffected by artificial cerebrospinal fluid (ACSF) (Figures 4F and S5E–S5G). These findings confirm that the 5-HT_3 and AMPA receptor activation of dopamine mesoaccumbens neurons by DR-SERT fibers enhances total dopamine levels in the nAcc. Although the presence of AMPA receptors on VTA dopamine neurons is well established, anatomical evidence for the expression of 5-HT_3 receptors in VTA dopamine neurons has not been reported, perhaps because of the lack of anti-5-HT_3 receptor antibodies capable of recognizing plasma membrane 5-HT_3 receptors (Morales et al., 1998). Therefore, we applied a combination of *in situ* hybridization (for detection of 5-HT_3 transcripts) and

TH immunolabeling, and we found expression of the functional subunit A (5-HT_{3A}) of the 5-HT_3 receptor in VTA TH-positive neurons (Figures 4G and 4G'). Within the VTA, we detected the expression of 5-HT_{3A} subunit primarily within the TH-positive neurons; more than 80% of neurons expressing the 5-HT_{3A} subunit were TH-positive neurons. However, only about one-third of the population of VTA TH-positive neurons coexpressed the 5-HT_{3A} subunit (Table S1), indicating that the postsynaptic effect of serotonin through the 5-HT_3 receptors is restricted to a subpopulation of dopamine neurons that innervate the nAcc.

Together, these results suggest (1) that VTA stimulation of DR inputs drives both serotonin and glutamate excitatory transmission on a particular subpopulation of VTA dopamine neurons, (2) that this transmission induces dopamine release in the nAcc, and (3) that this increase in dopamine release is mediated by activation of 5-HT_3 and AMPA receptors.

VTA Optical Activation of SERT Fibers Promotes CPP

Although some studies have reported that photoactivation of DR-serotonin neurons reinforces instrumental behavior (Li et al., 2016; Liu et al., 2014), others have reported that photoactivation of DR-serotonin neurons does not have a role in reward-seeking behavior (Fonseca et al., 2015; McDevitt et al., 2014). However, DR activation of serotonin neurons may result in global release of serotonin in many brain structures and activation of multiple serotonin receptors, leading to conflicting results. To overcome those limitations, we evaluated the behavioral consequences of selective VTA photoactivation of inputs from DR-SERT neurons because the VTA contains mesolimbic dopamine neurons shown to have a crucial role in reward and motivational function (Wise, 2004). We first evaluated neuronal coexpression of eYFP with tryptophan hydroxylase (TPH) by immunofluorescence microscopy in the DR of SERT-ChR2-eYFP mice (Figures 5A and S6). We found that all eYFP-positive neurons coexpressed TPH, and most DR TPH-positive neurons coexpressed eYFP (96.3% of TPH neurons coexpressed eYFP; n = 2,371 neurons from three mice), indicating the specific expression of ChR2-eYFP within DR serotonin neurons. We detected within the VTA abundant fibers (SERT inputs) from the DR eYFP-positive neurons (Figures 5B and 5B').

To evaluate the behavioral consequences of VTA activation of SERT fibers, we tested SERT-ChR2-eYFP mice in a three-chamber apparatus in which they received trains of optical stimulation when they entered the laser-paired chamber (Figures 5C and 5D). Mice were able to terminate the stimulation by crossing back to the connecting chamber. SERT-eYFP (control) mice spent equal time in both laser-paired and non-laser-paired chambers, whereas SERT-ChR2-eYFP mice spent significantly more time in the laser-paired chamber (Figure 5D). When we subsequently tested SERT-ChR2-eYFP mice in the absence of laser stimulation, we found that they spent more time in the chamber in which they had previously received the stimulation (Figures 5D and S6A–S6D; $p < 0.05$ versus nonpaired chamber; Newman-Keuls *post hoc* test). Thus, SERT-ChR2-eYFP mice not only earned the stimulation by entering the stimulation chamber when the stimulation was available but also acquired a preference for the stimulation chamber, as reflected by the time spent on the subsequent day when the stimulation was no longer available. VTA optical activation of SERT fibers of SERT-ChR2-eYFP mice did not alter locomotor activity (Figures S6B, S6E,

and S6F; p = 0.302, two-way ANOVA; n = 10). We next evaluated the effects of intra-VTA application of 5-HT_3, serotonin type 2 receptor (5-HT_2; receptor present on VTA dopamine neurons; Doherty and Pickel, 2000) or AMPA receptor antagonists on CPP induced by VTA optical activation of SERT inputs. We injected ondansetron (3 μg/0.3 μL), 5-HT_2 receptor antagonist ketanserin (0.5 μg/0.3 μL), or CNQX (1 μg/0.3 μL) into the VTA of SERT-ChR2-eYFP mice 10 min before the laser-paired training (Figure 5E). Although ACSF-injected mice showed a preference for the laser-paired chamber during both laser-paired training day and test day (Figure 5F), ondansetron- or CNQX-injected mice no longer preferred the laser-paired chamber during the laser-paired training day or the test day (Figures 5F and S6D). In ketanserin-injected mice, we observed a decrease in the preference for the laser-paired chamber during both laser-paired training day and test day, but it did not reach the level of significance. These results suggest that VTA 5-HT_3 and AMPA receptors have a critical role in the acquisition of CPP induced by the activation of VTA inputs from DR-SERT neurons.

Optical Activation of Either SERT Fibers or VGluT3 Fibers in the VTA Induces CPP of Different Durations

We have previously demonstrated that VTA activation of inputs from DR-VGluT3 neurons induces CPP mediated by the release of glutamate on mesoaccumbens dopamine neurons (Qi et al., 2014). Here, we compared the CPP induced by VTA optical stimulation of DR-SERT fibers and those induced by VTA optical stimulation of DR-VGluT3 fibers (Figures 6 and S7). For optical stimulation of DR-VGluT3 fibers, we drove expression of ChR2 tethered to eYFP in DR-VGluT3 neurons by injecting a viral vector encoding Cre-dependent ChR2 in the DR of neurons of VGluT3:: Cre mice (referred to here as VGluT3-ChR2-eFYP mice; Figure 6B). We confirmed that both SERT-ChR2-eYFP and VGluT3-ChR2-eYFP mice spent significantly more time in the laser-paired chamber. However, SERT-ChR2-eYFP mice spent less time in the laser-paired chamber (during the 2 days of training; 51% on training day 1 and 51% on training day 2, p = 0.000001, three-way ANOVA, n = 10) than did VGluT3-ChR2-eYFP mice (65% on training day 1 and 70% on training day 2; p = 0.012 on training day 1; p = 0.0002 on training day 2 versus the SERT-ChR2-eYFP mice; Newman-Keuls *post hoc* test) (Figure 6B). After 2 days of laser-paired training, we tested SERT-ChR2-eYFP and VGluT3-ChR2-eYFP mice for several days without laser stimulation (1, 4, 7, and 12 days after the last training day) to determine the duration of the preference elicited by the laser stimulation. We found that the time spent by SERT-ChR2-eYFP mice in the laser-paired chamber was stable for 1 wk. In contrast, the time spent by the VGluT3-ChR2-eYFP mice in the laser-paired chamber gradually and significantly decreased after each test day (Figure 6B; p < 0.01 versus training day 2; Newman- Newman-Keuls *post hoc).* These results indicate that, although DR-SERT and -VGluT3 inputs to VTA induce CPP, the rewarding effects mediated by SERT inputs are less, but they have longer duration.

DISCUSSION

Although investigated for more than 50 years, the role of serotonin in reward has remained controversial. We hypothesize that serotonin's role in reward depends on its individual pathways and synaptic characteristics. Here, we demonstrate that (1) DR-serotonin neurons provide both serotonin-only inputs, which establish *symmetric* synapses, and serotonin-

glutamate inputs, which establish *asymmetric* synapses within the VTA; (2) axon terminals from dual serotonin-glutamate neurons establish *asymmetric* synapses on VTA-dopamine neurons that innervate the nAcc; and (3) the release of serotonin and glutamate from DR to VTA, through the actions of glutamate and serotonin receptors, evokes nAcc release of dopamine, is reinforcing, and establishes CPP.

Selective VTA Cellular Targeting by DR Serotonin-Only and Dual Serotonin-Glutamate Neurons

The regulation of VTA dopamine neurons by serotonin has been the subject of debate for several decades. It is often suggested that VTA dopamine neurons are tonically inhibited by serotonin because the firing rate of VTA-putative dopamine neurons is increased in brains depleted of serotonin by chemicals or in brains with DR electrolytic lesions (Guiard et al., 2008; Hervé et al., 1979). In contrast, the increase of serotonin levels by peripheral administration of the serotonin reuptake inhibitor fluoxetine causes a dose-dependent inhibition of the firing rate of putative dopamine neurons in the VTA (Prisco and Esposito, 1995). Although interpretations of findings across these studies are hindered because of the multiple projections of the serotonergic system that are affected by global brain manipulation of serotonin levels and the lack of evidence of recorded neurons as being dopaminergic, we provide evidence supporting a model in which DR projections from SERT-positive neurons to VTA through the release of serotonin and glutamate exert excitatory actions on identified mesoaccumbens dopaminergic neurons.

The VTA is a major target of DR serotonin neurons (Bobillier et al., 1976; Hervé et al., 1987; Pierce et al., 1976; Van Bockstaele et al., 1994). However, recent tracing studies have demonstrated that DR serotonin-only, VGluT3-only, and dual serotonin-VGluT3 neurons target the VTA in the rat (Geisler et al., 2007; Hioki et al., 2010; Qi et al., 2014) and in the mouse (Qi et al., 2014). Although it has been assumed that the major input from DR to VTA is from serotonin neurons, we have previously shown that, within the total population of DR neurons innervating the VTA, a major population consists of VGluT3-only neurons (≈46%) with minor populations from serotonin-only (≈13%) or dual VGluT3-serotonin neurons (≈14%) (Qi et al., 2014). Here, we analyzed the frequency of axon terminals from both SERT-only and SERT-VGluT3 neurons in mouse VTA and found that SERT-only axon terminals were twice as frequent as the SERT-VGluT3 axon terminals. Although both SERT-only and SERT-VGluT3 neurons establish synapses on dopamine and nondopamine neurons, SERT-VGluT3 neurons more frequently synapse on dopamine neurons, and SERT-only neurons more frequently synapse on nondopamine neurons (Figures 7A and 7B). Given that, in addition to dopamine neurons, the VTA has glutamate-only, γ-amino-butyric acid (GABA)-only and dual glutamate-GABA neurons (Root et al., 2018), it remains to be determined the extent to which these different subpopulation of VTA neurons correspond to the nondopamine neurons targeted by SERT-only or SERT-VGluT3 neurons. In addition to long-range connections, the VTA GABA and glutamate neurons establish local synapses (Morales and Margolis, 2017; Zhang et al., 2015), whose activity may be differentially regulated by SERT-only or SERT-VGluT3 inputs, as reflected by our *in vivo* VTA recordings showing both neuronal excitation and neuronal inhibition evoked by VTA optical stimulation of SERT fibers.

We found that, irrespective of their postsynaptic target, the SERT terminals establishing *asymmetric* synapses coexpress VGluT3, and those establishing *symmetric* synapses lack VGluT3 (Figures 7A and 7B). Previous studies have characterized serotonergic synapses within the VTA as inhibitory or excitatory based exclusively on the symmetry or asymmetry of their synaptic membrane specializations (Morales and Pickel, 2012). Moreover, there is a prevailing view that *asymmetric* synapses are excitatory because of their postsynaptic excitatory serotonergic receptors, and conversely, *symmetric* synapses are inhibitory because of their postsynaptic inhibitory serotonergic receptors (Doherty and Pickel, 2000). Although we cannot discount the possibility that different types of postsynaptic serotonin receptors may be selectively expressed in *asymmetric* or *symmetric* synapses, our ultrastructural findings indicate that serotonergic axons terminals making *asymmetric* synapses coexpress VGluT3 protein, having the capability to co-release serotonin and glutamate. Thus, we propose that the excitatory nature of VTA serotonergic axons establishing *asymmetric* synapses is mediated, in part, by the presynaptic release of glutamate (from VGluT3-containing vesicles) and the presence of postsynaptic glutamatergic receptors.

In Vivo Electrophysiological Recordings and the Role of DR in Reward

Emerging electrophysiological evidence suggests that different DR neurons have different roles in reward-related processes (Bromberg-Martin et al., 2010; Miyazaki et al., 2011; Nakamura et al., 2008; Ranade and Mainen, 2009). Recordings of genetically identified DR serotonin neurons from head-restrained mice have shown that most DR serotonin neurons are tonically activated after reward-predicting cues in a cue-reward association task (Liu et al., 2014). Other studies, also from head-restrained mice, have shown that nearly 40% of DR serotonin neurons exhibit slow and subtle variations in their activity that correlate with the amount of reward in the environment (Cohen et al., 2015). Additional findings have shown that many DR serotonin neurons signal short-term information about upcoming rewards and punishments with brief changes in firing rates, leading to the suggestion that DR serotonin neurons signal reward and punishment on both slow and fast time scales (Cohen et al., 2015). To minimize stress induced by head-restraining, which may contribute to alterations in signaling by serotonin neurons (Luo et al., 2016), the activity of DR-serotonin neurons has been recorded in free-moving mice by both fiber photometry and single-cell recordings (Li et al., 2016). Photometry detection of changes in intracellular calcium showed that DR-serotonin neurons respond to both reward expectation and reward consumption (Li et al., 2016). Moreover, nearly 60% of the DR-serotonin neurons increase their firing rate tonically when mice are anticipating the reward and fire phasically after receipt of the reward, when multiple, single-unit recordings are employed (Li et al., 2016). These findings from DR-identified serotonin neurons indicate heterogeneity in their activity patterns in reward-related processes, but it remains to be determined which of the recorded patterns correspond to serotonin-only or serotonin-glutamate neurons, the brain area in which they project, and the nature of the postsynaptic neurons.

Photoactivation of DR-serotonin neurons has been recently applied to determine their role in reward-associated tasks (Fonseca et al., 2015; Li et al., 2016; Liu et al., 2014; McDevitt et al., 2014; Miyazaki et al., 2014). Findings from those studies have shown that photoactivation of DR-serotonin neurons promotes patience for future rewards (Fonseca et

al., 2015; Miyazaki et al., 2014) and reinforces (Li et al., 2016; Liu et al., 2014) or fails to reinforce instrumental behavior (Fonseca etal., 2015; McDevitt et al., 2014). It is unclear whether the discrepancy on the reinforcing effects may reflect differences in experimental conditions leading to activation of different classes of DR-serotonin neurons or serotonin receptors involved in different behaviors (Calizo et al., 2011; Hale and Lowry, 2011; Kiyasova et al., 2011). Because DR activation of serotonin neurons may result in global release of serotonin in many brain structures (Ren et al., 2018) and activation of multiple serotonin receptors, leading to conflicting results, we studied the specific ultrastructural and functional properties of DR serotonin fibers within the VTA. We found that most DR serotonin fibers synapsing on VTA dopamine neurons co-release glutamate, that some of those dopamine neurons target the nAcc, and that they are excited by DR dual serotonin-glutamate inputs through glutamate and serotonin receptors, excitation that results in the rapid release of dopamine in the nAcc (Figure 7C). Furthermore, mice learn to associate the effect of the VTA photostimulation of those DR serotonin-glutamate inputs with their environment, and subsequently, those mice exhibit a CPP for that environment (as animals remember the place at which they obtained such stimulation and return to it, despite the absence of the stimulation). Although acquisition of CPP induced by VTA optical activation of DR-SERT inputs is mediated by glutamate and serotonin receptors, future studies are needed to determine the roles that specific neurons within the DR pathway to VTA may have in different aspects of reward signaling. Within the VTA, in addition to the serotonin-glutamate *asymmetric* synapses on dopamine neurons, we found the serotonin-only terminal making *symmetric* synapses mostly on nondopaminergic neurons. It remains to be determined the nature of those nondopamine neurons and their serotonin receptor composition. Importantly, recent findings indicate that the rewarding effects observed after DR-serotonin neuron stimulation are reduced in knockout mice depleted of VGluT3 and are eliminated after DR chemical inhibition of serotonin production (Liu et al., 2014). These findings underscore the participation of both serotonin and glutamate in the reward-signaling ability of DR-serotonin neurons (Liu et al., 2014).

STAR⋆METHODS

CONTACT FOR REAGENT AND RESOURCE SHARING

Further information and requests for resources and reagents should be directed to and will be fulfilled by the Lead Contact, Marisela Morales (mmorales@intra.nida.nih.gov).

EXPERIMENT MODEL AND SUBJECT DETAILS

Mice—C57BL/6J mice were purchased from Jackson laboratories. Serotonin transporter (SERT)::Cre mice were purchased from Mutant Mouse Regional Resource Centers and were breed in the NIDA/IRP animal facility, and offspring mice were genotyped by PCR using primers to detect the presence of the Cre recombinase gene sequence (5′-CGG CAAACG GAC AGA AGC ATT-3′) and the presence of serotonin transporter solute carrier family 6 member 4 (Slc6a4) (5′-GGT CCT TGG CAG ATG GGC AT-3′). All animal procedures were performed in accordance with the National Institutes of Health Guidelines, and approved by the National Institute on Drug Abuse Animal Care and Use Committee.

Mice for anatomical studies: Eight male serotonin transporter (SERT)::Cre mice (8–12 weeks were injected Cre-inducible recombinant adeno-associated virus (AAV) vector to genetically target channelrhodopsin2 (ChR2) expression to serotonin neurons in the dorsal raphe nucleus (DR) of male adult SERT::Cre mice. SERT::Cre mice were injected in the DR (bregma: AP −4.2, ML ± 0.2, DV −3.4 to the skull surface) with AAV encoding ChR2 tethered to mCherry (SERT-ChR2-mCherry) or eYFP (SERT-ChR2-eYFP). Five weeks after viral injection into the DR, 4 of the SERT-ChR2-mCherry mice were iontophoretically injected into nAcc with the retrograde tract tracer Fluoro-Gold (FG; 1% in cacodylate buffer, pH 7.5) through a stereotaxically positioned glass micropipette by applying 3 mA current in 5 s pulses at 10 s intervals for 15 min (coordinates in mm relative to bregma: AP +1.4, ML ± 0.8, DV −4.8/−4.2). The micropipette was left in place for an additional 10 min to prevent tracer backflow up the injection track after each injection. Four male C57BL/6J mice (8–12 weeks), SERT::Cre mice at 6 weeks after virus injection or 1 week after FG injection were deeply anesthetized with chloral hydrate (35 mg/100 g) and perfused transcardially with fixative solution [4% paraformaldehyde (PFA) in 0.1 M phosphate buffer (PB, pH 7.3) supplemented with 0.15% glutaraldehyde and 15% picric acid in 0.1 M PB for fluorescent and electron microscopy or 4% PFA for *in situ* hybridization-immunohistochemistry]. For fluorescent and electron microscopy, brains were left in fixative solution for 2 h at 4°C, 2% PFA overnight at 4°C, rinsed with PB, and midbrains were cut into coronal serial sections (40 mm thick) with a vibratome (VT1000S, Leica, Vienna, Austria). For *in situ* hybridization-immunohistochemistry, rat brains were left in 4% PFA for 2 h at 4°C, rinsed with PB and transferred sequentially to 12%, 14% and 18% sucrose solutions in PB, and VTA coronal serial cryo-sections of 12 μm in thickness were prepared. All animals of the same sex of mixed genotypes were housed in groups of up to four animals per cage in an animal room at 22°C under a 12 h light/dark cycle (light on at 7 am), with *ad libitum* access to food and water.

Mice for electrical stimulation and optogenetic studies: For electrical stimulation studies, fifteen male C57BL/6J mice (8–12 weeks) were used. For optogenetic studies, eighty-six male SERT::Cre mice were injected in the DR with AAV-ChR2 tethered to mCherry (SERT-ChR2-mCherry mice), eYFP (SERT-ChR2-eYFP mice), or AVV encoding eYFP (SERT-eYFP mice). Ten male VGluT3::Cre mice were injected in the DR with AAV-ChR2 tethered to eYFP (VGluT3-ChR2-eYFP mice). Mice were positioned in a stereotaxic frame under anesthesia with isoflurane (3% isoflurane in 1L/min O_2 for induction and 2% for maintenance). Two small burr holes were drilled bilaterally over the DR at the coordinates in mm relative to bregma: AP −4.2, ML ± 0.2, DV −3.4 to the skull surface. A NanoFil syringe was used to deliver bilaterally 0.3 μl of virus (3×10^{12} genomes/ml) into the DR at a speed of 0.1 μl/min. For microdialysis study, six male C57BL/6J, eighteen SERT-ChR2-eYFP mice were implanted unilaterally with a microinjection guide cannula 1 mm above the VTA (AP −3.4, ML +0.3, DV −3.3) and a microdialysis guide cannula above the nAcc (AP +1.3, ML +0.6, DV −3.8). Mice were allowed to recover from surgery for 7 days before microdialysis. Mice for behavioral experiments were implanted 4–6 weeks after virus injection with a unilateral chronic optical fiber (200 μm diameter) or guide cannula directed above the VTA. These mice were allowed at least 10 day recovery before behavioral test. After *in vivo* studies, brain sections were obtained for location examination of injection or implantation.

Mice with incorrect virus injection, cannula or probe implantation were excluded from data analysis. Animal procedures were approved by the NIDA and the UMBI Animal Care and Use Committees.

Virus—Double-floxed reverse orf EF-1α::ChR2-eYFP, EF-1α-eYFP or double-floxed reverse of EF-1α::ChR2-mCherry cassettes were packaged in AAV vectors, serotyped with AAV1 or AAV5 coat proteins and packaged (3×10^{12} genomes/ml) by the UNC vector core (University of North Carolina, NC) or by the NIDA/IRP optogenetics and transgenic technology core.

METHOD DETAILS

Fluorescence microscopy and three-dimensional analysis—Free floating coronal vibratome sections were incubated for 1 h in PB supplemented with 4% bovine serum albumin (BSA) and 0.3% Triton X-100. Sections were then incubated with cocktails of primary antibodies: mouse anti-tryptophan hydroxylase antibody (T0678; Sigma-Aldrich, St. Louis, MO, USA, 1:500 dilution); guinea pig anti-VGluT3 antibody (135204; Synaptic System, 1:500 dilution) + rabbit anti-SERT antibody (HTT-Rb-Af560–1; Frontier Institute Co. Ltd, 1:250 dilution) + mouse anti-synaptophysin antibody (MAB368; MilliporeSigma, Billerica, MA,1:250 dilution); or mouse anti-TH antibody (MAB318; MilliporeSigma, 1:1000 dilution) + goat anti-GFP antibody (GFP-Go-Af1480; Frontier Institute Co. Ltd, 1:2000 dilution) + rabbit anti-FG antibody (AB153; MilliporeSigma, 1:2000 dilution) + guinea pig anti-VGluT3 antibody (135204; Synaptic System, 1:500 dilution) overnight at 4°C. After rinsing 3 × 10minin PB, sections were incubated inAlexa Fluor 594-affiniPure donkey anti-mouse (715–585-151; Jackson Immunoresearch Laboratories, West Grove, PA, USA, 1:100 dilution); a cocktail of Alexa Fluor 488-AffiniPure donkey anti-guinea pig (706–545-148; Jackson Immunoresearch Laboratories, 1:100 dilution) + Alexa Fluor 594-AffiniPure donkey anti-rabbit (711–585-152; Jackson Immunoresearch Laboratories Inc., 1:100 dilution) + Alexa Fluor 647-AffiniPure donkey anti-mouse (715–605-151; Jackson Immunoresearch Laboratories Inc., 1:100 dilution); or a cocktail of Dylight 405-AffiniPure donkey anti-mouse (715–475-150; Jackson Immunoresearch Laboratories, 1:100 dilution) + Alexa Fluor 488-AffiniPure donkey anti-goat (705–545-147; Jackson Immunoresearch Laboratories, 1:100 dilution) + Alexa Fluor 594-AffiniPure donkey anti-rabbit (711–585-152; Jackson Immunoresearch Laboratories, 1:100 dilution) + Alexa Fluor 647-AffiniPure donkey anti-guinea pig (706–605-148; Jackson Immunoresearch Laboratories, 1:100 dilution) for 2 h at room temperature. After rinsing, sections were mounted on slides and air-dried. Fluorescent images were collected with Olympus FV1000 Confocal System (Olympus, Center Valley, PA). Images were taken sequentially with different lasers with 100 × oil immersion objectives and z axis stacks were collected at 0.2 μm. The confocal images were collected from 4 mice (64 × 64 × 10 μm for each image, 50 images from each mouse). Given that both SERT and VgluT3 are detectable in axons and axon terminals, we used synaptophysin detection to label and quantified axon terminals expressing SERT or VGluT3. We obtained z stacks of confocal images (immunolabeled for detection of synaptophysin, SERT and VGluT3), and processed them with the Imaris microscopy software (Bitplane Inc., South Windsor, CT) to obtain three-dimensional quantification of axon terminals expressing synaptophysin with SERT-alone or with SERT-VGluT3. The same confocal

images were analyzed with the Amira microscopy software (ThermoFisher Scientific, Waltham, MA) to obtain three-dimensional reconstruction of putative synapses.

Electron microscopy—Vibratome tissue sections were rinsed with PB, incubated with 1% sodium borohydride in PB for 30 min to inactivate free aldehyde groups, rinsed in PB, and then incubated with blocking solution [1% normal goat serum (NGS), 4% BSA in PB supplemented with 0.02% saponin] for 30 min. Sections were then incubated with primary antibodies as follows: guinea pig anti-VGluT3 + rabbit anti-SERT + mouse anti-TH antibodies (triple labeling), or mouse anti-mCherry (632543; Takara, 1:1000 dilution) + guinea pig anti-VGluT3 + rabbit anti-TH (AB152, MilliporeSigma, 1:1000 dilution) (triple labeling), or mouse anti-mCherry + guinea pig anti-VGluT3 + rabbit anti-Fluoro-Gold antibodies (triple labeling). All primary antibodies were diluted in PB with 1% NGS, incubations were for 24 h at 4°C. Sections were rinsed and incubated overnight at 4°C in the corresponding secondary antibodies: biotinylated goat anti-rabbit antibody (PK-4001; for SERT detection) + anti-mouse IgG coupled to 1.4 nm gold (2001; Nanoprobes Inc., 1:100 dilution for TH detection) + anti-guinea pig IgG Fab' fragment coupled to 1.4 nm gold (for VGluT3 detection), or biotinylated horse anti-mouse antibody (PK-4002; for mCherry detection) + anti-guinea pig IgG Fab' fragment coupled to 1.4 nm gold (2055; Nanoprobes Inc., Stony Brook, NY, 1:100 dilution for VGluT3 detection) + anti-rabbit IgG coupled to 1.4 nm gold (2003; Nanoprobes Inc., 1:100 dilution forTH or Fluoro-Gold detection). Sections were rinsed in PB, and then in double-distilled water, followed by silver enhancement of the gold particles with the Nanoprobe Silver Kit (2012; Nanoprobes Inc., Stony Brook, NY) for 7 min at room temperature. Next, sections were incubated in avidin-biotinylated horseradish peroxidase complex (PK-4000 ABC kit; Vector Labs, Burlingame, CA,1:100 dilution) in PB for 2 h at room temperature and washed in PB. Peroxidase activity was detected by placing the sections in a solution containing 0.025% 3, 3 diaminobenzidine-4 HCl (DAB) and 0.003% hydrogen peroxide (H_2O_2) in PBfor 5–10 min. Sections were rinsed with PB and fixed with 0.5% osmium tetroxide in PBS for 25 min, washed in PBS followed by double-distilled water and then contrasted in freshly prepared 1% uranyl acetate for 35 min. Sections were dehydrated through a series of graded alcohols and with propylene oxide. Afterward, they were flat embedded in Durcupan ACM epoxy resin (14040; Electron Microscopy Sciences, Fort Washington, PA). Resin-embedded sections were polymerized at 60°C for 2 days. Sections of 65 nm were cut from the outer surface of the tissue with an ultramicrotome UC7 (Leica Microsystems Inc., Buffalo Grove, IL) using a diamond knife (Diatome, fort Washington, PA). The sections were collected on formvar-coated single slot grids and counterstained with Reynolds lead citrate. Sections were examined and photographed using a Tecnai G^2 12 transmission electron microscope (Fei Company, Hillsboro, OR) equipped with a digital micrograph OneView camera (Gatan Inc., Pleasanton, CA). Specificity of primary antibodies has been previously described(Zhang etal., 2015).

Slice preparation and electrophysiology—Male SERT-ChR2-eYFP mice were used to detect DR glutamatergic inputs on VTA mesoaccumbens dopamine neurons (n = 9) as well as DR serotonin inputs on VTA dopamine neurons (n = 4). For detection of DR glutamatergic inputs on VTA mesoaccumbens dopamine neurons, SERT-ChR2-eYFP mice

(six weeks after virus injection) were bilaterally injected in the nAcc shell with 0.5% cholera toxin B subunit (CTb) conjugated with Alexa Fluor® 594 (CTb-594, Life technologies, C34777). Two to three weeks after the CTb injection, mice were deeply anesthetized with isoflurane and decapitated. Brains were removed and tranferred to oxygenated (95% O_2/5% CO_2), ice-cold N-Methyl-D-glucamin (NMDG)-based cutting solution (in mM: 93 NMDG, 2.5 KCl, 10 $MgSO_4$, 0.5 $CaCl_2$,1.2 NaH2PO4, 30 $NaHCO_3$, 25 glucose, 20 HEPES, 5 sodium ascorbate, 3 sodium pyruvate; PH 7.2–7.4). Horizontal slices containing VTA (200 μM) were then obtained using a vibratome (VT1200, Leica). Slices were first incubated in the NMDG-based solution at 34°C for 12 min, then transferred and maintained in artificial CSF (aCSF; in mM: 126 NaCl, 3 KCl, 1.5 $MgCl_2$, 2.4 $CaCl_2$,1.2 NaH_2PO_4, 26 $NaHCO_3$,11 glucose) at room temperature. During recording, a midbrain slice was transferred to a heated chamber (32°C) and perfused with oxygenated aCSF (2 ml/min). Slice was visualized under an upright microscope equipped with differential interference contrast (DIC) optics (BX51WI, Olympus). VTA CTb labeled neurons found close to the medial terminal nucleus of the accessory optical tract (MT) were recorded. Cell-attached and whole-cell recordings were performed using MultiClamp 700B (Molecular Devices) amplifier. Recording electrodes (3~5 MΩ) were filled with a standard internal solution (in mM: 140 K-gluconate, 2 NaCl, 1.5 $MgCl_2$, 10 HEPES, 0.1 EGTA, 4 Mg-ATP, 0.3 Na-GTP, 10 Tris-phosphocreatine, pH 7.2, 290 mOSM) supplemented with 0.2% biocytine. This K-gluconate-based low Cl^- internal solution preserves cell body TH-protein during the whole-cell recording, thus we can identify dopamine neurons reliably by immunohistochemistry(Margolis et al., 2010). A 200 μm core optical fiber, coupled to a diode-pumped solid-state laser, was positioned just above the slice and aimed at the recording area to deliver 473 nm optical stimulation (3–5 ms pulses, 5–8 mW). Drugs were diluted and applied through the perfusion aCSF. Slices were fixed after recording with 4% PFAover night at 4°C. Slices were incubated with mouse anti-TH (1:500, EMD Millipore, MAB318) primary antibody for over 2 nights at 4°C. After rinse in PB, slices were incubated with DyLight 405 AffiniPure Donkey Anti-Mouse IgG (715–475-151; Jackson ImmunoResearch Laboratories, 1:200 dilution) and Cy5 Streptavidin (016–170-084; Jackson ImmunoResearch Laboratories, 1:500 dilution) over night at 4°C. Florescent images were taken with Olympus FV1000 confocal microscope. For detection of DR serotoninergic inputs on VTA dopamine neurons, VTA DA neurons were first identified by their location relative to the MT, interpeduncular fossa and medial lemniscus. Additionally, cells satisfied the following electrophysiological criteria: hyperpolarization-activated inward current (Ih), 1–5 Hz firing frequency, action potential half-width ≥ 1.5 ms, spike frequency adaptation and spike failure during prolonged injection of depolarizing current(Goertz et al., 2015). The presence of Ih is a partial predictor of dopaminergic identity for cells in the VTA(Margolis et al., 2006). Recording pipettes had a tip resistance between 3–7 MOhm and were filled with (in mM): 135 CsCl, 2 $MgCl_2$,10 HEPES, 5 QX-314, 5 EGTA, 2 Na-ATP, 0.2 Na-GTP. Cells were voltage clamped at −60 mV and EPSCs were evoked using a 200 μm optical fiber coupled to a 473 nm laser or with a 250μm tungsten bipolar electrode. The optical fiber was placed within the bath and aimed at the site of recording, and was used to deliver optical stimulation of 1mW intensity. To test the use of optical stimulation in measuring paired-pulse ratios of EPSCs, we verified that increasing light intensity and pulse duration caused a decrease in onset latency with an increase in amplitude. Increasing light intensity and pulse

duration augments afferent fiber recruitment, thus increasing EPSC amplitude and decreasing onset latency. This suggests that at lower intensity and pulse duration optogenetic stimulation evokes EPSCs via propagating action potentials(Tecuapetla et al., 2010). The bipolar electrode for electrical stimulation was used to deliver 0.5 ms pulses. Following a 10-minute stable baseline period, 5-HT currents were blocked by bath application of 1 μM Y-25130 (5-HT_3 receptor antagonist) and data were collected for a minimum 10 minutes. To quantify the effect of Y-25130, sweeps were averaged for the last 5 minutes of the pre- and post-drug phases of the experiment.

***In vivo* electrophysiology—**Male SERT-ChR2-eYFP mice (n = 6) were anesthetized with urethane (1.4 g/kg, i.p.), and mounted in a stereotaxic frame. A hole was drilled in the skull to access VTA. Glass micropipettes (6–10 MU) filled with 2.0% Pontamine Sky Blue (BDH Chemicals, Poole, England) in 3M NaCl were used for recordings. Glass electrodes were utilized to shield against any potential light-induced artifacts that can be observed with metal electrode recordings alone(Cardin et al., 2010). A 100 μm core multimode fiber was glued 350 μm dorsal to the glass electrode tip, and the fiber was connected to a 473 nm DPSS laser (OEM laser systems, Bluffdale, UT). Signals were amplified using a Neuro Data IR283A (Cygnus Technology, Delaware Water Gap, PA) and BrownLee 440 amplifier. Neuronal activity was bandpass filtered between 300 Hz and 3000 Hz. The biopotentials were digitized using a Power 1401 Analog-Digital Converter (Cambridge Electronic Design, Cambridge UK). Spontaneously active or optogenetically-driven neurons were recorded and analyzed. VTA recordings were obtained between −3.1 to −3.5 mm AP, 0 to 0.5 mm ML and −4.2 to −4.6 mm DV. Entrance into the VTAwasdemarked by passage through a layer of fast firing neurons dorsal to the VTA. Neurons were randomly sampled by slowly lowering the micropipette through the VTA. Baseline activity was recorded for 3 to 5 min, DR fibers were activated for 6 s at 20 Hz with 5 mW 4 ms light pulses. Peristimulus time histograms were constructed at 500 ms resolution bins, with a window width of 6 s before and 12 s after the stimulus onset. PSTHs were analyzed to determine excitatory and inhibitory responses. The 6 s before the stimulation were compared with the 6 slight stimulation using theWilcoxon signed-rank test. Signal to noise ratio were typically >5:1. After recordings, animals were perfused with 4% PFA, DR and VTA cryosections (30 μm) were prepared to verify the deposit of the pontamine sky in the recording sites and the expression of ChR2-eYFP in cell body and terminals. Neurons recorded external to the VTA were excluded from the analysis

***In vivo* electrical stimulation and fast scan cyclic voltammetry (FSCV)—**Male C57BL/6J mice (n = 15) were positioned in a stereotaxic frame under anesthesia with urethane (1.5 g/kg weight). A carbon fiber microelectrode (glass-encased, T-650 carbon fiber, 6 μm diameter with 100–120 μm exposed length, Amoco Corporation, Greenville, SC, USA) was implanted in the nucleus accumbens core (coordinates in mm relative to bregma: AP +1.2, ML +1.1, DV −3.7 to the brain tissue surface). A bipolar stimulating electrode was implanted in the ipsilateral DR (coordinates in mm relative to bregma: AP −4.2, ML +0.2, DV −3.4). An Ag/AgCl wire that served as the reference electrode was implanted into the contralateral hemisphere. Extracellular levels of dopamine in the nAcc core were monitored by *in vivo* FSCV in response to 60 Hz for 2 s electrical stimulation (biphasic stimulating pulses, 4 ms and 300 μA each phase) of the DR, parameters previously shown to induce 5-

HT release in the midbrain(Hashemi et al., 2009). For FSCV, a triangular waveform from −0.4 V to +1.3 V and back to −0.4 V at 400 V/s (versus the implanted Ag/AgCl reference electrode) was applied through the carbon fiber electrode. Stimulation-evoked release of dopamine was recorded during and after DR stimulation, and selectivity for the detected dopamine signal was verified by intraperitoneal (i.p.) injection of a D_2 receptor antagonist (eticlopride, 2 mg/kg), that augmented the signal. The selective serotonin reuptake inhibitor fluoxetine (10 mg/kg) was also systemically injected to determine the possible contribution of serotonin to the recorded signal. While the cyclic voltammograms for norepinephrine and dopamine are similar, norepinephrine is unlikely to be a significant contributor to the signal because dopamine-β-hydroxylase is not detectable in this region(Baldo et al., 2003). At the end of each experiment, the site of stimulation was marked by passing 20 s DC anodal current of 300 μA. Carbon fiber microelectrodes were calibrated *in vitro* with a solution of dopamine (1 μM).

The participation of serotonin type (5-HT_3) receptors in the release of dopamine in the nAcc core in response to DR electrical stimulation was initially tested by i.p. injection of ondansetron (5-HT_3 receptors antagonist, 2 mg/kg). Four baseline voltammograms were taken before and after DR electrical stimulation prior to ondansetron injection. Fifteen minutes after injection, additional voltammograms were recorded at 5 min intervals during and after DR electrical stimulation fora total period of 45 min, followed by injection of eticlopride (2 mg/kg, i.p.) to confirm the nature of the recorded signals. The participation of VTA5-HT_3 and AMPA receptors in the release of dopamine in the nAcc core evoked by DR electrical stimulation was tested by VTA microinjections (3 μg/0.3 μl) of ondansetron or the AMPA receptor antagonist CNQX. Dopamine oxidation currents were transformed to concentration using a flow injection system that delivered a square pulse of 1 μM. A guide cannula was implanted above the VTA, and an Ag/AgCl wire was implanted into the contralateral hemisphere. A 33-gauge microinjector was inserted 0.5 mm below the tip of the guide cannula. The infusion lasted 1 min using a microprocessor-controlled infusion pump. The microinjector was removed at 1 min after infusion, and accumbal dopamine release was measured by FSCV in 5 minutes, and every 5 min during and after DR electrical stimulation for a total period of 25 min. Dopamine selectivity of the recorded signal was verified by FSCV measurement of accumbal dopamine evoked 15 min after eticlopride injection (2 mg/kg, i.p.), monitored every 5 min during and after DR electrical stimulation for a period of 15 min.

***In vivo* optical stimulation and FSCV—**Six to eight weeks after virus injection, SERT-ChR2-mCherry mice (n = 8; 4 mice for optical stimulation of DR neurons and 4 mice for optical stimulation of VTA serotonergic inputs) were positioned in a stereotaxic frame under anesthesia with urethane. A 10 mm longitudinal incision on the skin in the dorsum of the cranium was made to perform a craniotomy, and allowing access to the DR or VTA. A 200 μm core optical fiber (Thorlabs, Newton, NJ) was inserted and a train of blue light (473 nm wavelengths, 20 mW, 4 ms duration/pulse, 120 pulses, 20 Hz) was delivered through the optical fiber. Extracellular dopamine in the nAcc core was monitored by FSCV (as describe for electrical stimulation) every 15 min during and after DR optical stimulation, and dopamine signal selectivity was verified by i.p. injection of eticlopride. Expression of ChR2-

mCherry was verified at the end of each experiment by fluorescent mCherry immunodetection.

***In vivo* optical stimulation, microdialysis and quantification of DA—**A microdialysis probe (0.24 × 1 mm, CMA7, CMA Microdialysis) was inserted into the guide cannula implanted in the nAcc of wild-type (n = 6) or SERT-ChR2-eYFP (n = 18) mice in the evening before testing. The inlet tubing of the probe was connected to a microinfusion pump (CMA 100) via a fiber-optic and liquid rotary joint (Doric Lenses), and animals were placed into chambers (20 × 30 × 35 cm). Probes were perfused with ACSF (in mM: 140 NaCl, 2.7 KCl, 1.2 MgCl2, 1.4 CaCl2, 5 glucose, adjusted to pH 7.3–7.4 using NaOH) overnight at a flow rate of 0.2 μl min-1. The following day, an optical fiber was inserted into the VTA through the guide cannula, and perfusate was replaced with fresh ACSF at the flow rate of 2.4 μl min-1. Following a 3-h equilibration period, microdialysis samples were collected every 10 min into 5 μl 0.1 M perchloric acid to prevent DA degradation. Three 10-min samples were collected to determine the baseline of DA release in nAcc. Optical stimulation was delivered via optical fiber into the VTA for 10 min (473 nm, 20 mW, 10 ms, 20 Hz, 3 s on/off). To test the involvement of VTA glutamate AMPA or 5-HT_{3A} receptors, after the optical stimulation, three consecutive samples were collected before microinjection with ACSF, CNQX (1 μg/0.2 μl), or ondansetron (3 μg/0.2 μl) (n = 6 each group) into the VTA. One 10 min sample was collected after the microinjection followed by another 10-min optical stimulation in the VTA. Three more consecutive samples were collected after the optical stimulation. DA concentration was measured by reverse-phase HPLC with electrochemical detection. Dialysate was injected into an Eicom HTEC-500 HPLC system containing a HPLC column (PP-ODS2, 4.6 × 30 mm), a HTEC-500 pump, and an integrated amperometric detector. The mobile phase consisted of (in mM) 100 NaH_2PO4, 1.3 EDTA, 2.0 decane-1-sulfonate, 0.5% methanol, pH 5.4. Applied potential was set at +400 mV versus Ag/AgCl. Concentration of dialysate DA levels were estimated using calibration curves obtained from external standards. Detection limit of DA using these conditions was approximately 50 pM.

Combination of *in situ* hybridization and immunolabeling—Coronal free-floating sections from 3 rats (12 μm in thickness) were processed as described previously(Wang and Morales, 2008). Brain sections were incubated for 10 min in PB containing 0.5% Triton X-100, rinsed 2 × 5 min with PB, treated with 0.2 N HCl for 10 min, rinsed 2 × 5 min with PB and then acetylated in 0.25% acetic anhydride in 0.1 M triethanolamine, pH 8.0 for 10 min. Sections were rinsed 2 × 5 min with PB, fixed with 4% PFA for 10 min. Prior to hybridization and after a final rinse with PB, the free-floating sections were incubated in hybridization buffer (50% formamide; 10% dextran sulfate; 5 × Denhardt's solution; 0.62 M NaCl; 50 mM DTT; 10 mM EDTA; 20 mM PIPES, pH 6.8; 0.2% SDS; 250 μg/ml salmon sperm DNA; 250 μg/ml tRNA) for 2 h at 55°C. Sections were hybridized for 16 h at 55°C in hybridization buffer containing [^{35}S]- and [^{33}P]-labeled single-stranded antisense or sense of rat 5-HT_{3A} (nucleotides104–1561, Accession # NM 024394.2) probes at 10^7 cpm/ml. Sections were treated with 4 μg/ml RNase A at 37°C for 1 h, washed with 1 × SSC, 50% formamide at 55°C for 1 h, and with 0.1 × SSC at 68°C for 1 h. After the last SSC wash, sections were rinsed with PB and incubated for 1 h in PB supplemented with 4% BSAand

0.3% Triton X-100. This was followed by the overnight incubation at 4°C with an anti-TH mouse monoclonal antibody (MAB318; EMD Millipore, 1:500 dilution). After rinsing 3 × 10 min in PB, sections were processed with an ABC kit (Vector Laboratories, Burlingame, CA). The material was incubated for 1 h at room temperature in a 1:200 dilution of the biotinylated secondary antibody, rinsed with PB, and incubated with avidin-biotinylated horseradish peroxidase for 1 h. Sections were rinsed and the peroxidase reaction was then developed with 0.05% DAB and 0.003% H_2O_2. Free-floating sections were mounted on coated slides. Slides were dipped in Ilford K.5 nuclear tract emulsion (Polysciences, Inc., Warrington; 1:1 dilution in double distilled water) and exposed in the dark at 4°C for four weeks prior to development.

CPP—SERT-ChR2-eYFP(n = 51), VGluT3-ChR2-eYFP (n = 10) and SERT-eYFP mice (n = 11) were used for behavior studies. A three-chamber CPP apparatus was used for the test (Anymaze, Wood Dale, IL), which consisted of two chambers (20 × 18 × 35 cm) with distinct walls drawings floor and shape, and a connecting chamber (20 × 10 × 35 cm). We recorded all animal movements via a CCD camera interfaced with a video tracking software. The CPP paradigm consisted of five or eight days. On each day, the mice were connected to an optical fiber and allowed to access three chambers freely. On habituation and pretest day (15 min sessions), the animals were allowed to explore the apparatus without optical stimulation. On laser conditioning days 1 and 2 (30 min sessions), we assigned one chamber as the laser-paired chamber (counterbalanced across all mice). The animals received optical stimulation (473 nm wavelength, 20 mW, 10 ms duration/pulse, 20 Hz) when they entered the laser-paired chamber. The stimulation continued until the animal left the laser-paired chamber. On test day (15 min session), the animals were allowed to explore the apparatus without optical stimulation. For the CPP comparison between SERT-ChR2-eYFP and VGluT3-ChR2-eYFP mice, we tested the mice in the absence of light 1 day (test 1), 4 days (test 2), 7 days (test 3) and 12 days (test 4) after laser conditioning day 2. The participation of VTA 5-HT_3, 5-HT_2, and AMPA receptors in CPP was tested by VTA microinjections of 5-HT_3 receptor antagonist ondansetron (3 μg/0.3 μl), 5-HT_2 receptor antagonist ketanserin (0.5 μg/0.3 μl) or the AMPA receptor antagonist CNQX (1 μg/0.3 μl). Intra-VTA microinjection of ACSF served as control. The infusion lasted 1min using a microprocessor-controlled infusion pump. The microinjector was removed 1 min after infusion, and CPP test was performed 10 min after injection.

Locomotor activity test—SERT-ChR2-eYFP (n = 10) were used to test locomotor activity in an open field apparatus (40 × 40 × 35 cm, Anymaze, Wood Dale, IL). The locomotor activity test paradigm consisted of five days. On each day, the mice were connected to an optical fiber and allowed to move freely in the chamber for 1 min, then followed by test session. Test session lasted 10 min and was divided into 10 60 s trials. During odd-numbered trials, continuous laser stimulation was given (473 nm wavelength, 10 mW, 10 ms duration/pulse, 20 Hz). During even-numbered trials, the laser stimulation remained off. Travel distance and speed of each trail were recorded via a CCD camera interfaced with ANY-maze behavior tracking software.

QUANTIFICATION AND STATISTICAL ANALYSIS

Ultrastructural analysis—Serial thin sections of VTA (bregma −2.92 mm to −3.88 mm) of the mouse brain atlas of Paxinosand Franklin, VTA (bregma −4.92mm to −6.48 mm) of the rat brain atlas of Paxinos and Watson were used in this study. Synaptic contacts were classified according to their morphology and immunolabel, and photographed at a magnification of 6800–13000 ×. The morphological criteria used for identification and classification of cellular components observed in these thin sections were as previously described (Peters et al., 1991). Type I synapses, here referred as asymmetric synapses, were defined by the presence of contiguous synaptic vesicles within the presynaptic axon terminal and a thick postsynaptic density (PSD) greater than 40 nm. Type II synapses, here referred as symmetric synapses, were defined by the presence of contiguous synaptic vesicles within the presynaptic axon terminal and a thin PSD(Zhang et al., 2015). Serial sections were obtained to determine the type of synapse. In the serial sections, a terminal containing greater than 5 immunogold particles were considered as immunopositive terminal. Pictures were adjusted to match contrast and brightness by using Adobe Photoshop (Adobe Systems Incorporated, Seattle, WA). The data were collected from 4 rats and 4 SERT::Cre mice. This experiment was successfully repeated three times. Electron microscopy and confocal analysis quantification occurred blindly.

Data analysis of TH cells co-expressing 5-HT_{3A} mRNA of Combination of *in situ* hybridization and immunolabeling—Sections were viewed, analyzed, and photographed with bright field or epiluminescence microscopy using an Olympus VS120 microscope. Single and double-labeled neurons were observed within each traced region at high power (20 × objective lens) and marked electronically. Subdivisions of the midbrain dopamine system were traced according to Phillipson(Phillipson, 1979a, b), Halliday &Törk(Halliday and Törk, 1986), German & Manaye(German and Manaye, 1993). A neuron was considered to express TH immunoreactivity when its soma was clearly labeled as brown. ATH immunolabeled neuron was included in the calculation of total population of TH cells when the stained cell was at least 5 μm in diameter. Pictures were adjusted to match contrast and brightness by using the program Adobe Photoshop (Adobe Systems Incorporated, Seattle, WA).

Statistical analysis—All the statistical analyses applied in fast scan cyclic voltammetry and electrophysiological studies were performed by paired t test, one-way ANOVA or two-way ANOVA when applicable. We performed two or three-way ANOVA to analyze the microdialysis and behavioral data when applicable. ANOVA was followed by a post hoc Newman–Keuls test for multiple comparisons. Statistical analyses were performed with STATISTICA 9 or GraphPad prism 5. $p < 0.05$ was considered significant.

Supplementary Material

Refer to Web version on PubMed Central for supplementary material.

ACKNOWLEDGMENTS

We thank Dr. Roy Wise for critical reading of the manuscript and Drs. David Barker and Stephan Steidl for advice on behavioral studies. The Intramural Research Program of the National Institute on Drug Abuse (NIDA/NIH) supported this work. J.F.C. was supported by NIDA grants DA022340 and DA042595. C.A.P. was supported by NIDA grant DA038453 and NIMH grants MH107229 and MH113341. J.A.G. was supported by NIDA grant DA041303. Resources for three-dimensional analysis were supported by NS050274.

REFERENCES

Alex KD, and Pehek EA (2007). Pharmacologic mechanisms of serotonergic regulation of dopamine neurotransmission. Pharmacol. Ther 113, 296–320. [PubMed: 17049611]

Baldo BA, Daniel RA, Berridge CW, and Kelley AE (2003). Overlapping distributions of orexin/hypocretin- and dopamine-beta-hydroxylase immuno-reactive fibers in rat brain regions mediating arousal, motivation, and stress. J. Comp. Neurol 464, 220–237. [PubMed: 12898614]

Bayer VE, and Pickel VM (1991). GABA-labeled terminals form proportionally more synapses with dopaminergic neurons containing low densities of tyrosine hydroxylase-immunoreactivity in rat ventral tegmental area. Brain Res. 559, 44–55. [PubMed: 1685938]

Bobillier P, Seguin S, Petitjean F, Salvert D, Touret M, and Jouvet M (1976). The raphe nuclei of the cat brain stem: a topographical atlas of their efferent projections as revealed by autoradiography. Brain Res. 113,449–486. [PubMed: 821589]

Boureau YL, and Dayan P (2011). Opponency revisited: competition and cooperation between dopamine and serotonin. Neuropsychopharmacology 36, 74–97. [PubMed: 20881948]

Bromberg-Martin ES, Hikosaka O, and Nakamura K (2010). Coding of task reward value in the dorsal raphe nucleus. J. Neurosci 30, 6262–6272. [PubMed: 20445052]

Calizo LH, Akanwa A, Ma X, Pan YZ, Lemos JC, Craige C, Heemstra LA, and Beck SG (2011). Raphe serotonin neurons are not homogenous: electrophysiological, morphological and neurochemical evidence. Neuropharmacology 61, 524–543. [PubMed: 21530552]

Cameron DL, Wessendorf MW, and Williams JT (1997). A subset of ventral tegmental area neurons is inhibited by dopamine, 5-hydroxytryptamine and opioids. Neuroscience 77, 155–166. [PubMed: 9044383]

Campbell AD, Kohl RR, and McBride WJ (1996). Serotonin-3 receptor and ethanol-stimulated somatodendritic dopamine release. Alcohol 13, 569–574. [PubMed: 8949951]

Cardin JA, Carlen M, Meletis K, Knoblich U, Zhang F, Deisseroth K, Tsai LH, and Moore CI (2010). Targeted optogenetic stimulation and recording of neurons in vivo using cell-type-specific expression of Channelrhodopsin-2. Nat. Protoc 5, 247–254. [PubMed: 20134425]

Carr DB, and Sesack SR (2000). Projections from the rat prefrontal cortex to the ventral tegmental area: target specificity in the synaptic associations with mesoaccumbens and mesocortical neurons. J. Neurosci 20,3864–3873. [PubMed: 10804226]

Cohen JY, Amoroso MW, and Uchida N (2015). Serotonergic neurons signal reward and punishment on multiple timescales. eLife 4, 4.

Cools R, Nakamura K, and Daw ND (2011). Serotonin and dopamine: unifying affective, activational, and decision functions. Neuropsychopharmacology 36, 98–113. [PubMed: 20736991]

Deakin JF (1980). On the neurochemical basis of self-stimulation with midbrain raphe electrode placements. Pharmacol. Biochem. Behav 13, 525–530. [PubMed: 6449012]

Di Giovanni G, Di Matteo V, Pierucci M, and Esposito E (2008). Serotonin-dopamine interaction: electrophysiological evidence. Prog. Brain Res 172, 45–71. [PubMed: 18772027]

Doherty MD, and Pickel VM (2000). Ultrastructural localization of the serotonin 2A receptor in dopaminergic neurons in the ventral tegmental area. Brain Res. 864, 176–185. [PubMed: 10802024]

Dray A, Gonye TJ, Oakley NR, and Tanner T (1976). Evidence for the existence of a raphe projection to the substantia nigra in rat. Brain Res. 113, 45–57. [PubMed: 953733]

Fletcher PJ, Ming ZH, and Higgins GA (1993). Conditioned place preference induced by microinjection of 8-OH-DPAT into the dorsal or median raphe nucleus. Psychopharmacology (Berl.) 113, 31–36. [PubMed: 7862825]

Fletcher PJ, Tampakeras M, and Yeomans JS (1995). Median raphe injections of 8-OH-DPAT lower frequency thresholds for lateral hypothalamic self-stimulation. Pharmacol. Biochem. Behav 52, 65–71. [PubMed: 7501680]

Fonseca MS, Murakami M, and Mainen ZF (2015). Activation of dorsal raphe serotonergic neurons promotes waiting but is not reinforcing. Curr. Biol 25, 306–315. [PubMed: 25601545]

Geisler S, Derst C, Veh RW, and Zahm DS (2007). Glutamatergic afferents of the ventral tegmental area in the rat. J. Neurosci 27, 5730–5743. [PubMed: 17522317]

German DC, and Manaye KF (1993). Midbrain dopaminergic neurons (nuclei A8, A9, and A10): three-dimensional reconstruction in the rat. J. Comp. Neurol 331, 297–309. [PubMed: 8514911]

Goertz RB, Wanat MJ, Gomez JA, Brown ZJ, Phillips PE, and Paladini CA (2015). Cocaine increases dopaminergic neuron and motor activity via midbrain alpha1 adrenergic signaling. Neuropsychopharmacology 40, 1151–1162. [PubMed: 25374094]

Guiard BP, El Mansari M, Merali Z, and Blier P (2008). Functional interactions between dopamine, serotonin and norepinephrine neurons: an in-vivo electrophysiological study in rats with monoaminergic lesions. Int. J. Neuropsychopharmacol 11, 625–639. [PubMed: 18205979]

Hale MW, and Lowry CA (2011). Functional topography of midbrain and pontine serotonergic systems: implications for synaptic regulation of serotonergic circuits. Psychopharmacology (Berl.) 213, 243–264. [PubMed: 21088958]

Halliday GM, and Törk I (1986). Comparative anatomy of the ventromedial mesencephalic tegmentum in the rat, cat, monkey and human. J. Comp. Neurol 252, 423–445. [PubMed: 3782510]

Hashemi P, Dankoski EC, Petrovic J, Keithley RB, and Wightman RM (2009). Voltammetric detection of 5-hydroxytryptamine release in the rat brain. Anal. Chem 87,9462–9471.

Hayes DJ, and Greenshaw AJ (2011). 5-HT receptors and reward-related behaviour: a review. Neurosci. Biobehav. Rev 85, 1419–1449.

Hervé D, Simon H, Blanc G, Lisoprawski A, Le Moal M, Glowinski J, and Tassin JP (1979). Increased utilization of dopamine in the nucleus accumbens but not in the cerebral cortex after dorsal raphe lesion in the rat. Neurosci. Lett 15, 127–133. [PubMed: 530523]

Hervé D, Pickel VM, Joh TH, and Beaudet A (1987). Serotonin axon terminals in the ventral tegmental area of the rat: fine structure and synaptic input to dopaminergic neurons. Brain Res. 435, 71–83. [PubMed: 2892580]

Higgins GA, and Fletcher PJ (2003). Serotonin and drug reward: focus on 5-HT2C receptors. Eur. J. Pharmacol 480, 151–162. [PubMed: 14623358]

Hioki H, Nakamura H, Ma YF, Konno M, Hayakawa T, Nakamura KC, Fujiyama F, and Kaneko T (2010). Vesicular glutamate transporter 3-expressing nonserotonergic projection neurons constitute a subregion in the rat midbrain raphe nuclei. J. Comp. Neurol 518, 668–686. [PubMed: 20034056]

Imperato A, and Angelucci L (1989). 5-HT3 receptors control dopamine release in the nucleus accumbens of freely moving rats. Neurosci. Lett 101, 214–217. [PubMed: 2549462]

Kapur S, and Remington G (1996). Serotonin-dopamine interaction and its relevance to schizophrenia. Am. J. Psychiatry 153, 466–476. [PubMed: 8599393]

Kirby LG, Zeeb FD, and Winstanley CA (2011). Contributions ofserotonin in addiction vulnerability. Neuropharmacology 61, 421–432. [PubMed: 21466815]

Kiyasova V, Fernandez SP, Laine J, Stankovski L, Muzerelle A, Doly S, and Gaspar P (2011). A genetically defined morphologically and functionally unique subset of 5-HT neurons in the mouse raphe nuclei. J. Neurosci 31, 2756–2768. [PubMed: 21414898]

Kranz GS, Kasper S, and Lanzenberger R (2010). Reward and the serotonergic system. Neuroscience 166, 1023–1035. [PubMed: 20109531]

Li Y, Zhong W, Wang D, Feng Q, Liu Z, Zhou J, Jia C, Hu F, Zeng J, Guo Q, et al. (2016). Serotonin neurons in the dorsal raphe nucleus encode reward signals. Nat. Commun 7, 10503. [PubMed: 26818705]

Liu ZH, and Ikemoto S (2007). The midbrain raphe nuclei mediate primary reinforcement via GABA(A) receptors. Eur. J. Neurosci 25, 735–743. [PubMed: 17328772]

Liu Z, Zhou J, Li Y, Hu F, Lu Y, Ma M, Feng Q, Zhang JE, Wang D, Zeng J, et al. (2014). Dorsal raphe neurons signal reward through 5-HT and glutamate. Neuron 81, 1360–1374. [PubMed: 24656254]

Lucki I (1998). The spectrum of behaviors influenced by serotonin. Biol. Psychiatry 44, 151–162. [PubMed: 9693387]

Luo M, Li Y, and Zhong W (2016). Do dorsal raphe 5-HT neurons encode “beneficialness”? Neurobiol. Learn. Mem 135, 40–49.

Margolis EB, Lock H, Hjelmstad GO, and Fields HL (2006). The ventral tegmental area revisited: is there an electrophysiological marker for dopaminergic neurons? J. Physiol 577, 907–924. [PubMed: 16959856]

Margolis EB, Coker AR, Driscoll JR, Lemaître AI, and Fields HL (2010). Reliability in the identification of midbrain dopamine neurons. PLoS ONE 5, e15222. [PubMed: 21151605]

McBride WJ, Lovinger DM, Machu T, Thielen RJ, Rodd ZA, Murphy JM, Roache JD, and Johnson BA (2004). Serotonin-3 receptors in the actions of alcohol, alcohol reinforcement, and alcoholism. Alcohol. Clin. Exp. Res 28, 257–267. [PubMed: 15112933]

McCabe C, Woffindale C, Harmer CJ, and Cowen PJ (2012). Neural processing of reward and punishment in young people at increased familial risk of depression. Biol. Psychiatry 72, 588–594. [PubMed: 22704059]

McDevitt RA, Tiran-Cappello A, Shen H, Balderas I, Britt JP, Marino RAM, Chung SL, Richie CT, Harvey BK, and Bonci A (2014). Serotonergic versus nonserotonergic dorsal raphe projection neurons: differential participation in reward circuitry. Cell Rep. 8, 1857–1869. [PubMed: 25242321]

Miliaressis E, Bouchard A, and Jacobowitz DM (1975). Strong positive reward in median raphe: specific inhibition by para-chlorophenylalanine. Brain Res. 08, 194–201.

Miyazaki KW, Miyazaki K, and Doya K (2011). Activation of the central serotonergic system in response to delayed but not omitted rewards. Eur. J. Neurosci 33, 153–160. [PubMed: 21070390]

Miyazaki KW, Miyazaki K, Tanaka KF, Yamanaka A, Takahashi A, Tabuchi S, and Doya K (2014). Optogenetic activation of dorsal raphe serotonin neurons enhances patience for future rewards. Curr. Biol 24, 2033–2040. [PubMed: 25155504]

Morales M, and Margolis EB (2017). Ventral tegmental area: cellular heterogeneity, connectivity and behaviour. Nat. Rev. Neurosci 18, 73–85. [PubMed: 28053327]

Morales M, and Pickel VM (2012). Insights to drug addiction derived from ultrastructural views of the mesocorticolimbic system. Ann. N Y Acad. Sci 1248,71–88. [PubMed: 22171551]

Morales M, Battenberg E, and Bloom FE (1998). Distribution of neurons expressing immunoreactivity for the 5HT3 receptor subtype in the rat brain and spinal cord. J. Comp. Neurol 402, 385–401. [PubMed: 9853906]

Müller CP, Carey RJ, Huston JP, and De Souza Silva MA (2007). Serotonin and psychostimulant addiction: focus on 5-HT1A-receptors. Prog. Neurobiol 81, 133–178. [PubMed: 17316955]

Nakamura K, Matsumoto M, and Hikosaka O (2008). Reward-dependent modulation of neuronal activity in the primate dorsal raphe nucleus. J. Neurosci 28, 5331–5343. [PubMed: 18480289]

Nestler EJ, and Carlezon WA Jr. (2006). The mesolimbicdopamine reward circuit in depression. Biol. Psychiatry 59, 1151–1159. [PubMed: 16566899]

Omelchenko N, and Sesack SR (2005). Laterodorsal tegmental projections to identified cell populations in the rat ventral tegmental area. J. Comp. Neurol 483, 217–235. [PubMed: 15678476]

Pessia M, Jiang ZG, North RA, and Johnson SW (1994).Actionsof5-hydroxytryptamine on ventral tegmental area neurons of the rat in vitro. Brain Res. 654, 324–330. [PubMed: 7987681]

Peters A, Palay SL, and Webster H.d. (1991). The Fine Structure of the Nervous System: Neurons and Their Supporting Cells, Third Edition (Oxford University Press).

Phillips AG, Carter DA, and Fibiger HC (1976). Differential effects of para-chlorophenylalanine on self-stimulation in caudate-putamen and lateral hypothalamus. Psychopharmacology (Berl.) 49, 23–27. [PubMed: 134387]

Phillipson OT (1979a). The cytoarchitecture of the interfascicular nucleus and ventral tegmental area of Tsai in the rat. J. Comp. Neurol 187, 85–98. [PubMed: 489779]

Phillipson OT (1979b). A Golgi study of the ventral tegmental area of Tsai and interfascicular nucleus in the rat. J. Comp. Neurol 187, 99–115. [PubMed: 489780]

Pierce ET, Foote WE, and Hobson JA (1976). The efferent connection of the nucleus raphe dorsalis. Brain Res. 107, 137–144. [PubMed: 1268717]

Poschel BP, and Ninteman FW (1971). Intracranial reward and the forebrain's serotonergic mechanism: studies employing para-chlorophenylalanine and para-chloroamphetamine. Physiol. Behav 7, 39–46. [PubMed: 4337925]

Poschel BP, Ninteman FW, McLean JR, and Potoczak D (1974). Intracranial reward after 5,6-dihydroxytryptamine: further evidence for serotonin's inhibitory role. Life Sci 15, 1515–1522. [PubMed: 4550011]

Prisco S, and Esposito E (1995). Differential effects of acute and chronic fluoxetine administration on the spontaneous activity of dopaminergic neurones in the ventral tegmental area. Br. J. Pharmacol 116, 1923–1931. [PubMed: 8528581]

Qi J, Zhang S, Wang HL, Wang H, de Jesus Aceves Buendia J, Hoffman AF, Lupica CR, Seal RP, and Morales M (2014). A glutamatergic reward input from the dorsal raphe to ventral tegmental area dopamine neurons. Nat. Commun 5, 5390. [PubMed: 25388237]

Ranade SP, and Mainen ZF (2009). Transient firing of dorsal raphe neurons encodes diverse and specific sensory, motor, and reward events. J. Neurophysiol 102, 3026–3037. [PubMed: 19710375]

Redgrave P, and Horrell RI (1976). Potentiation of central reward by localised perfusion of acetylcholine and 5-hydroxytryptamine. Nature 262, 305–307. [PubMed: 958379]

Ren J, Friedmann D, Xiong J, Liu CD, Ferguson BR, Weerakkody T, DeLoach KE, Ran C, Pun A, Sun Y, et al. (2018). Anatomically defined and functionally distinct dorsal raphe serotonin sub-systems. Cell 175, 472–487. [PubMed: 30146164]

Rompre PP, and Miliaressis E (1985). Pontine and mesencephalic substrates of self-stimulation. Brain Res. 359, 246–259. [PubMed: 4075148]

Root DH, Zhang S, Barker DJ, Miranda-Barrientos J, Liu B, Wang HL, and Morales M (2018). Selective brain distribution and distinctive synaptic architecture of dual glutamatergic-gabaergic neurons. Cell Rep. 23, 3465–3479. [PubMed: 29924991]

Ruf BM, and Bhagwagar Z (2009). The 5-HT1B receptor: a novel target for the pathophysiology of depression. Curr. Drug Targets 10, 1118–1138. [PubMed: 19702551]

Shin R, and Ikemoto S (2010). The $GABA_B$ receptor agonist baclofen administered into the median and dorsal raphe nuclei is rewarding as shown by intracranial self-administration and conditioned place preference in rats. Psychopharmacology (Berl.) 208, 545–554. [PubMed: 20054525]

Simon H, Le Moal M, and Cardo B (1976). Intracranial self-stimulation from the dorsal raphe nucleus of the rat: effects of the injection of para-chlorophenylalanine and of alpha-methylparatyrosine. Behav. Biol 16, 353–364. [PubMed: 132167]

Tecuapetla F, Patel JC, Xenias H, English D, Tadros I, Shah F, Berlin J, Deisseroth K, Rice ME, Tepper JM, and Koos T (2010). Glutamatergic signaling by mesolimbic dopamine neurons in the nucleus accumbens. J. Neurosci 30, 7105–7110. [PubMed: 20484653]

Trent F, and Tepper JM (1991). Dorsal raphé stimulation modifies striatal-evoked antidromic invasion of nigral dopaminergic neurons in vivo. Exp. Brain Res. 84, 620–630. [PubMed: 1830848]

Tsai CT (1989). Involvement of serotonin in mediation of inhibition of substantia nigra neurons by noxious stimuli. Brain Res. Bull 23, 121–127. [PubMed: 2529952]

Van Bockstaele EJ, Cestari DM, and Pickel VM (1994). Synaptic structure and connectivity of serotonin terminals in the ventral tegmental area: potential sites for modulation of mesolimbic dopamine neurons. Brain Res. 647, 307–322. [PubMed: 7522922]

Van Der Kooy D, Fibiger HC, and Phillips AG (1978). An analysis of dorsal and median raphe self-stimulation: effects of parachlorophenylalanine. Pharmacol. Biochem. Behav 8, 441–445. [PubMed: 149989]

Vengeliene V, Bilbao A, Molander A, and Spanagel R (2008). Neuropharmacology of alcohol addiction. Br. J. Pharmacol 154, 299–315. [PubMed: 18311194]

Wang HL, and Morales M (2008). Corticotropin-releasing factor binding protein within the ventral tegmental area is expressed in a subset of dopaminergic neurons. J. Comp. Neurol. 509, 302–318. [PubMed: 18478589]

Watson JM, and Dawson LA (2007). Characterization of the potent 5-$HT_{1A/B}$ receptor antagonist and serotonin reuptake inhibitor SB-649915: preclinical evidence for hastened onset of antidepressant/anxiolytic efficacy. CNS Drug Rev. 13, 206–223. [PubMed: 17627673]

Wise RA (2004). Dopamine, learning and motivation. Nat. Rev. Neurosci 5, 483–494. [PubMed: 15152198]

Zhang S, Qi J, Li X,Wang HL, Britt JP, Hoffman AF, Bonci A, Lupica CR, and Morales M (2015). Dopaminergic and glutamatergic microdomains in a subset of rodent mesoaccumbens axons. Nat. Neurosci 18, 386–392. [PubMed: 25664911]

Ziauddeen H, and Murray GK (2010). The relevance of reward pathways for schizophrenia. Curr. Opin. Psychiatry 23, 91–96. [PubMed: 20051858]

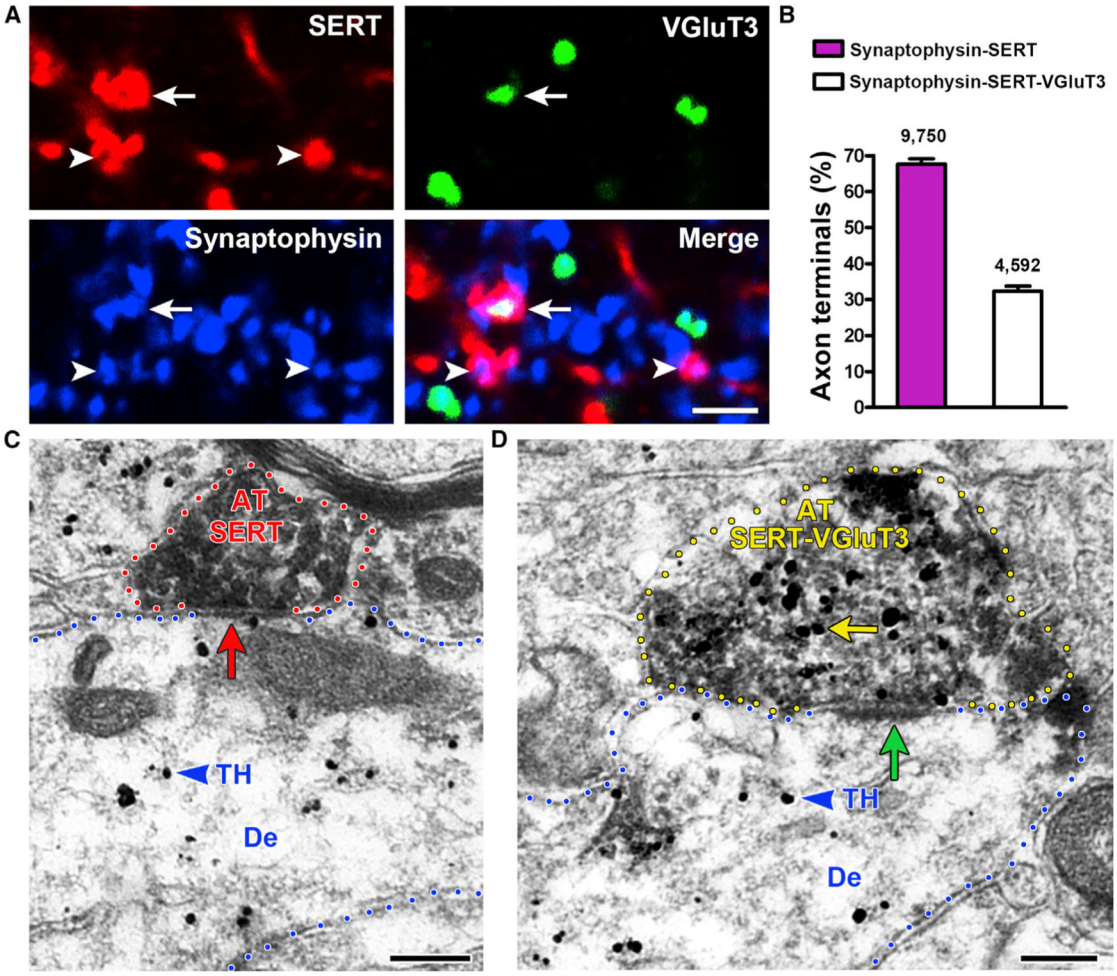

Figure 1. Both SERT-Only and SERT-VGluT3 Neurons Synapse on VTA TH Neurons

(A) VTA detection of SERT (red), VGluT3 (green), or synaptophysin (blue). Synaptophysin terminals with SERT (arrowheads) or SERT-VGluT3 (arrow).

(B) VTA frequency of synaptophysin-SERT and synaptophysin-SERT-VGluT3 terminals; bars represent means ± SEM (four mice, 14,342 counted terminals; 67.66% ± 1.43% synaptophysin-SERT and 32.34% ± 1.43% synaptophysin-SERT-VGluT3). Paired t test, $t_{(3)} = 12.33$, $p = 0.0011$.

(C and D) SERT-only (C) or SERT-VGluT3 (D) axon terminals (AT) make synapses on VTA TH-positive neurons. Triple immunolabeling: TH label (gold particles, blue arrowheads); SERT-immunoperoxidase label (scattered dark material) and VGluT3 label (gold particles, yellow arrow).

(C) SERT AT lacking VGluT3 (red outline) makes a symmetric synapse (red arrow) with a TH dendrite (De).

(D) SERT-VGluT3 AT (yellow outline) makes an asymmetric synapse (green arrow) with a TH dendrite.

Scale bars: 2 μm (A) and 200 nm (C and D).

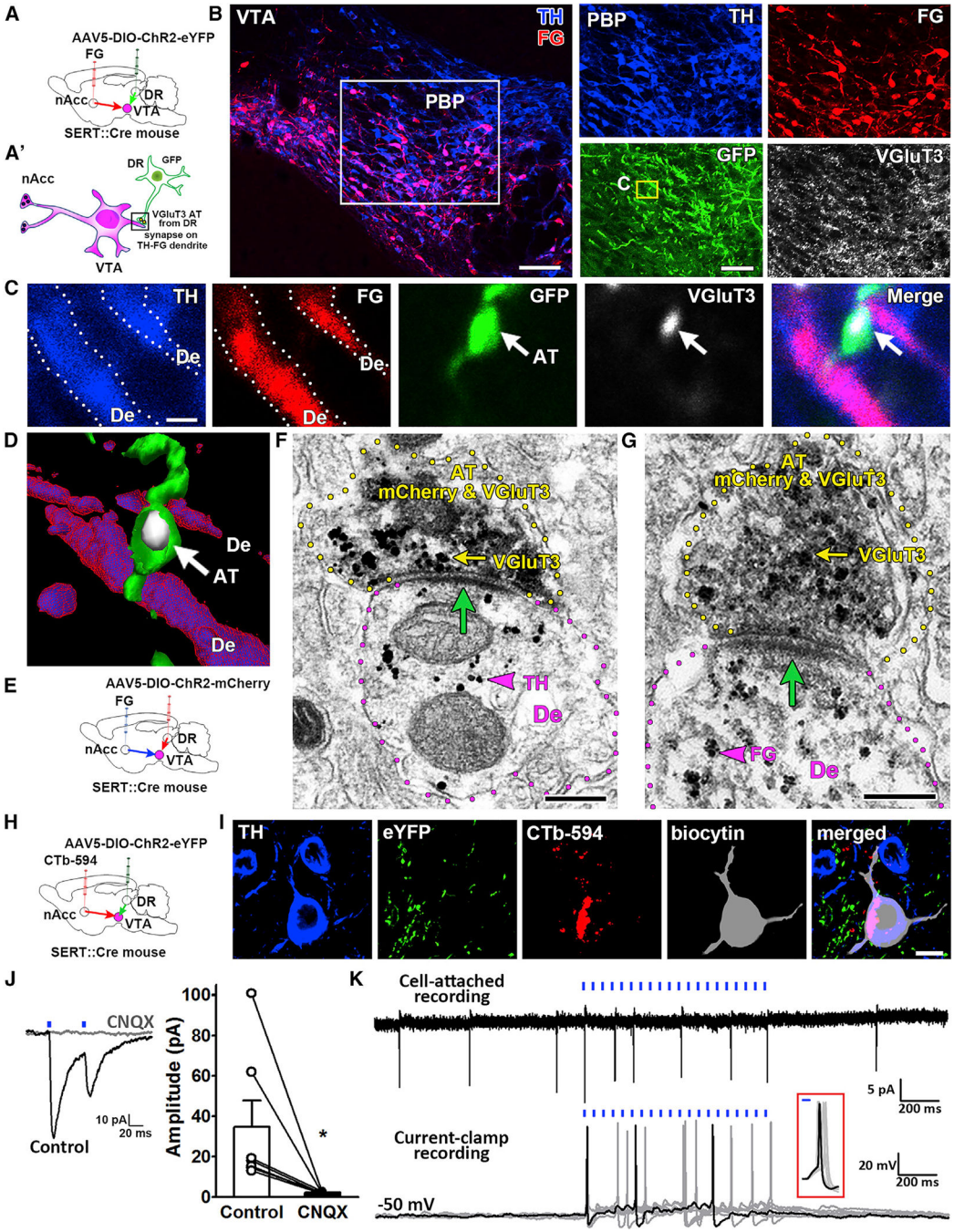

Figure 2. SERT-VGluT3 Axon Terminals from DR Make Excitatory Synapses on VTA TH Neurons that Target the nAcc

(A) Double-injected SERT::Cre mice, AAV5-DIO-ChR2-eYFP in DR and retrograde tracer Fluoro-Gold (FG) in nAcc.

(A') Schematic representation of a VTA dopamine neuron projecting to nAcc (mesoaccumbens neuron) making an asymmetric synapse with a SERT-VGluT3 axon terminal.

(B-D) VTA confocal microscopy. (B) Detection of TH (blue), FG (red), GFP (green), and VGluT3 (far-red) in VTA of double-injected SERT::Cre mice. TH-FG (mesoaccumbens)

neurons are seen as magenta; yellow rectangle seen at higher magnification in (C) showing a dendrite (De) from a TH-FG neuron adjacent to an eYFP-VGluT3 input (white-arrows) from DR-SERT neuron.

(D) Association between the TH-FG dendrite and SERT-VGluT3 terminal (white-arrow) is better seen after a three-dimensional reconstruction of confocal images. Bregma at −3.40 mm. PBP, parabrachial pigmented area.

(E-G) VTA electron microscopy.

(E) Double-injected SERT::Cre mice, AAV5-DIO-ChR2-mCherry in DR and FG in nAcc.

(F and G) Axon terminals (AT, yellow outlines) from DR SERT neurons (mCherry-immunoperoxidase label; scattered dark material) coexpressing VGluT3 (gold particles, yellow arrow) make asymmetric synapses (green arrow) on dendrites (magenta outlines). SERT-VGluT3 terminal makes asymmetric synapses (green arrow) on TH-dendrite De, TH, gold particle indicated by magenta arrowhead in (F) or on a FG-dendrite (FG, gold particle indicated by magenta arrowhead in (G).

(H) Double-injected SERT::Cre mice, AAV5-DIO-ChR2-eYFP in DR and CTb-594 in nAcc.

(I) Whole-cell recorded CTb-neuron in lateral VTA neurons confirmed as TH-neurons.

(J) Paired-pulse optical stimulation evoked EPSC was blocked by CNQX (20 μM) (control, 34.8 ± 12.8 pA; CNQX, 2.1 ± 0.2 pA; n = 7, paired t test, $t_{(6)} = 2.561$, *p = 0.043).

(K) Cell-attached and current-clamp recordings showing increase of VTA neuronal firing by 20-Hz local optical stimulation. Inset: Expanded current-clamp recordings show synchronization of the first action potential driven by the optical stimulation.

Scale bars: 100 μm in (B), left; 50 μm in (B), right; 1 μm in (C); 200 nm in (F and G); and 10 μm in (I).

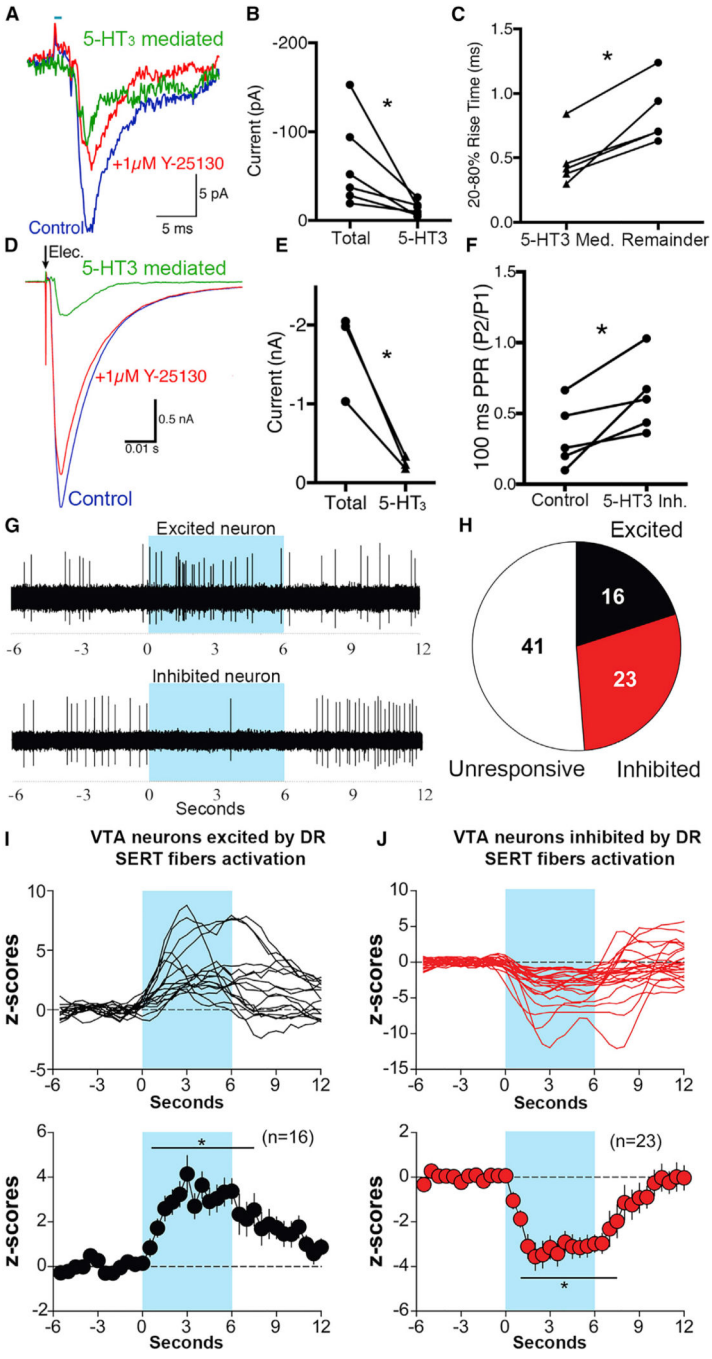

Figure 3. VTA Optical Stimulation of SERT Terminals Expressing ChR2 Evokes 5-HT3 Mediated EPSCs on Dopamine Neurons

(A-F) VTA slice electrophysiological recordings.

(A) Whole-cell recording of a VTA DA neuron during optical stimulation of DR inputs before (blue) and after (red) blocking 5-HT3 receptors. In green is the current mediated by 5-HT3 receptors (red trace subtracted from blue trace).

(B) Summarized data of the total current and the current mediated by 5-HT3 receptors from optical stimulation (paired t test, $t_{(5)} = 3.432$, *p = 0.019, n = 6).

(C) Summarized difference in rise time between the 5-HT3-mediated current from optical stimulation and the current remaining after 5-HT3 receptor blockade (*, significantly different from remainder, one-way repeated-measures ANOVA, $F_{2,8} = 16.72$, *p = 0.0014; n = 5).

(D) Whole-cell recording of a VTA DA neuron and electrical stimulation inputs before (blue) and after (red) blocking 5-HT3 receptors. In green is current mediated by 5-HT3 receptors.

(E) Summarized total current and current mediated by 5-HT3 receptors from electrical stimulation (paired t test, $t_{(2)} = 4.848$, *p = 0.04, n = 3).

(F) Blocking 5-HT3 receptors changes the paired pulse ratio from optical stimulation (paired t test, $t_{(4)} = 3.2$, *p = 0.033, n = 5). Data are represented as every data point of nine cells from four different animals.

(G and H) Activation of DR inputs evokes excitation or inhibition of VTA neurons.

(G) Original recording of VTA, with top trace showing an excited neuron, and bottom trace showing an inhibited neuron. Blue bars indicate the duration of photoactivation of DR fibers within the VTA.

(H) Proportion of evoked neural responses.

(I) VTA neurons excited by DR-SERT input activation. Top shows responses of individual neurons, and bottom shows population average (*, significantly different from prestimulation, one-way repeated-measures ANOVA, Greenhouse-Geisser corrected, $F_{4,61} = 5.55$, p = 0.00065; Neuman-Keuls *post hoc* test, *p < 0.05; see p value at each time point in Table S2).

(J) VTA neurons inhibited by photoactivation of DR-SERT fibers. Top shows responses of individual neurons, and bottom shows population average (*, significantly different from prestimulation, one-way repeated-measures ANOVA, Greenhouse-Geisser corrected, $F_{4,81} = 10.16$, p = 0.000001; Neuman-Keuls *post hoc* test, *p<0.05; seep value at each time point in Table S2). Blue bars indicate the duration of photoactivation of DR.

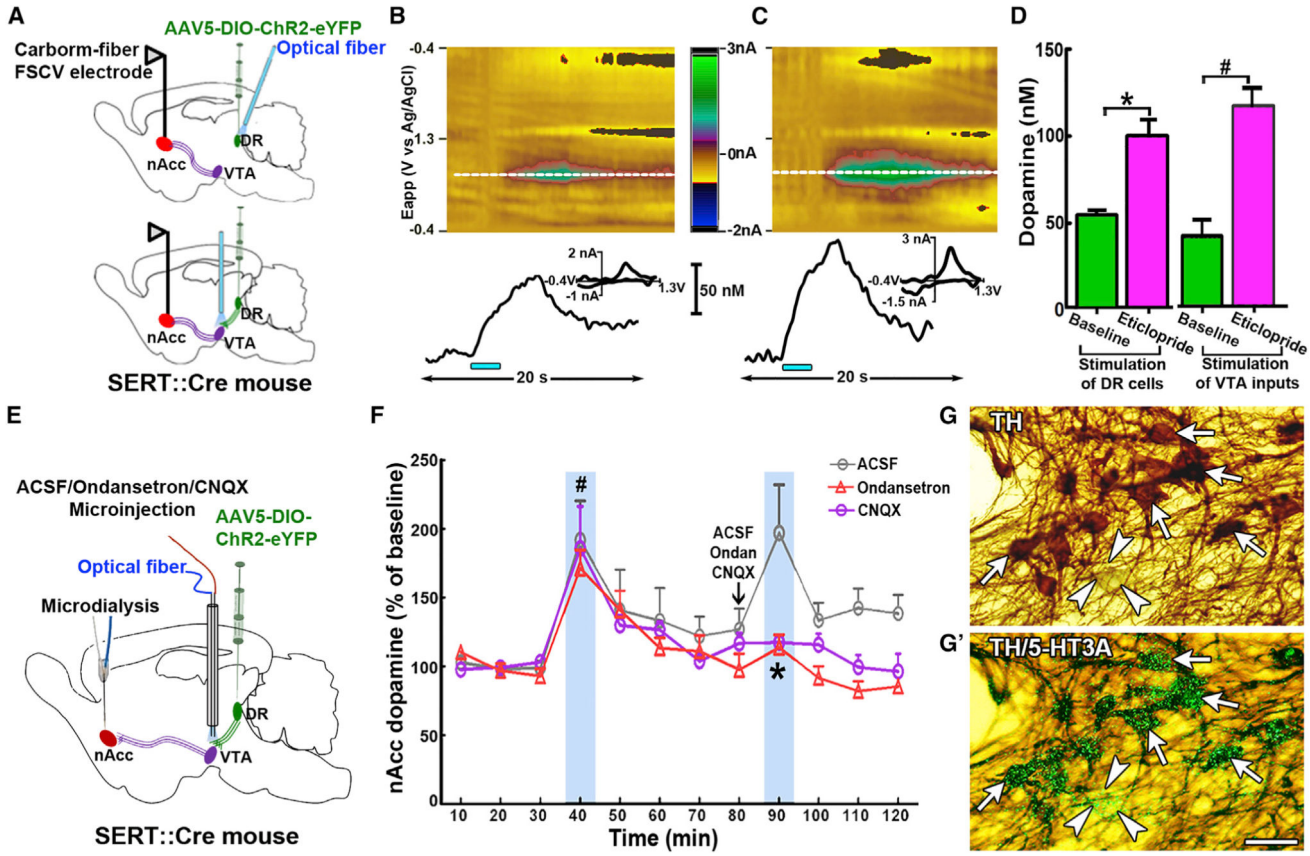

Figure 4. Optical Stimulation of DR-SERT Neurons or VTA-SERT Inputs Evokes Release of Dopamine in nAcc Core

(A) DR viral injection in SERT::Cre mice and optical stimulation of DR-SERT neurons (top) or VTA DR-SERT fibers (bottom) and fast scan cyclic voltammetry (FSCV) record in nAcc.

(B) Color plot (top) and dopamine concentration trace (bottom) show nAcc core dopamine release evoked by DR optical stimulation (6 s, 473 nm, 20 mW, 4 ms duration/pulse, 20 Hz). Inset illustrates characteristic dopamine voltammogram.

(C) Systemic administration of eticlopride increased release of dopamine in nAcc core evoked by DR optical stimulation confirming the recorded signal as dopamine. Top: Eticlopride treatment (2 mg/kg, i.p.) increased release of dopamine induced by DR optical stimulation. Bottom: Corresponding trace indicates the concentration of dopamine (nM) in response to DR optical stimulation after peripheral administration of eticlopride. Inset illustrates characteristic dopamine voltammogram. Optical stimulation onset at 5 s is indicated by blue bars in (B) and (C).

(D) Eticlopride significantly increased release of dopamine in nAcc elicited by optical stimulation of DR-SERT neurons or VTA-SERT inputs from DR. The significant difference from baseline (green bars) is indicated by * or # (Student's t test, $t_{(3)} = 5.61$, *p = 0.011, stimulation of SERT neurons [pink bar], n = 4; $t_{(3)} = 3.96$, #p = 0.029, stimulation SERT-inputs [pink bar], n = 4).

(E) Viral injection in DR of SERT::Cre mice, intra-VTA microinjection of 5-HT_{3A} receptor antagonist ondansetron or AMPA receptor antagonist CNQX, VTA optical stimulation of DR inputs, and microdialysis in nAcc.

(F) VTA optical activation of DR-SERT inputs induces nAcc dopamine release that was abolished by intra-VTA microinjection of ondansetron or CNQX. Each point represents a 10-min dialyzate sampling period (means ± SEM percentage of dopamine baseline, n = 6 each group); blue rectangles indicate the period of optical stimulation. Two-way ANOVA indicates main-effect time: $F_{11,165} = 11.95$, $p = 0.000001$; group × time interactions: $F_{22,165} = 1.69$, $p = 0.0334$. The 40-min time-point samples were significantly different from all the baseline time-point samples (#$p < 0.05$, Newman-Keuls *post hoc* test [see p value at each time point in Table S2]; ACSF group: 191.9% ± 28.5%; ondansetron group: 171.3% ± 13.4%; CNQX group: 185.7% ± 30.6%). A single intra-VTA microinjection of ondansetron or CNQX significantly reduced the enhanced nAcc DA levels elicited by light stimulation. The 90-min time-point samples from ondansetron group and CNQX group were significantly different from the ones in the ACSF group (*$p = 0.0062$, ondansetron versus ACSF; *$p = 0.0086$, CNQX versus ACSF, Newman-Keuls *post hoc* test; ACSF group: 196.9% ± 35.0%; CNQX group: 117.5% ± 4.0%; ondansetron group: 113.7% ± 9.4%). (G and G') Expression of 5-HT_{3A} mRNA in VTA TH neurons. TH-positive neurons (arrows) are shown in (G). TH signal is seen as brown (G and G') and 5-HT_{3A} mRNA signal appears as aggregates of green grains (G') (n = 3). Arrows indicate examples of neurons coexpressing TH and 5-HT_{3A} mRNA. Arrowheads indicate an example of a neuron expressing 5-HT_{3A} mRNA but lacking TH. Scale bar: 30 μm.

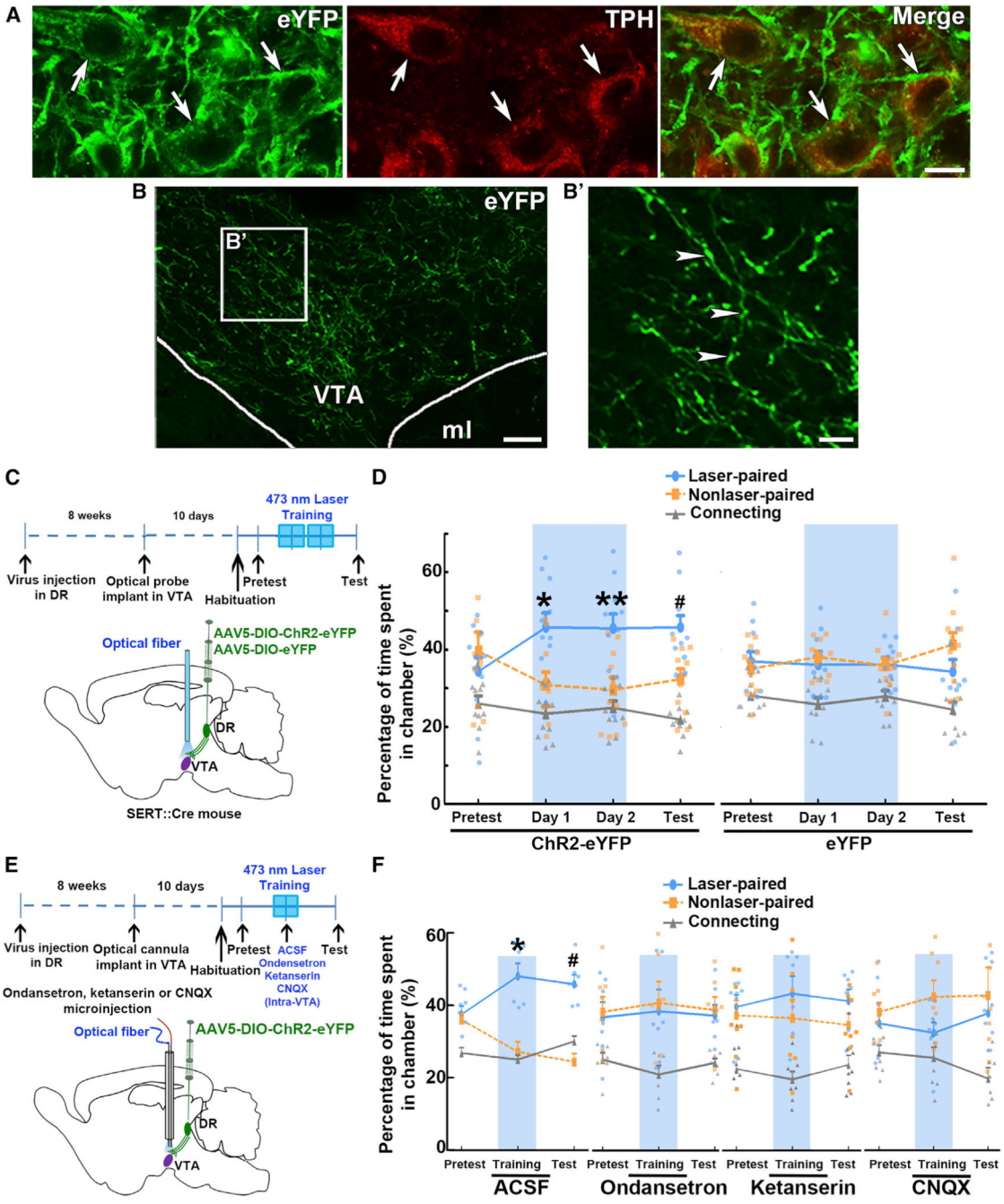

Figure 5. VTA Optical Stimulation of DR Inputs Containing ChR2 under the SERT Promoter Promotes Conditioned Place Preference

(A) Expression of ChR2-eYFP in DR serotonin neurons under the regulation of the SERT promoter (SERT::Cre mice). Confocal images showing cell-specific ChR2-eYFP expression (green) in DR serotonin (tryptophan hydroxylase [TPH]) neurons (red).

(B) Confocal images of ChR2-eYFP-positive axons (green, arrowheads) present in the VTA region. (B') is a closer view of the box in (B). ml, medial lemniscus.

(C) Diagram showing experimental timeline (top) and diagram of virus injection in the DR of SERT::Cre mice and VTA optical stimulation of DR SERT terminals (bottom).

(D) SERT-ChR2-eYFP, but not SERT-eYFP, mice spent more time in the chamber in which VTA optical stimulation was given during training days. On the test day, SERT-ChR2-eYFP mice also spent more time in the chamber in which optical stimulation was given on previous days. Relative time spent in each chamber is represented as means ± SEM (n = 11 each group). Blue rectangles indicate optical stimulation available in the laser-paired chamber. SERT-ChR2-eYFP mice showed preference for laser-associated chamber on two laser-paired training days and on test day in comparison with non-laser-associated chamber (day × chamber × group interaction: $F_{6, 120} = 2.717$, p = 0.016, three-way ANOVA; *p = 0.01, **p = 0.005, #p = 0.036, Newman–Keuls *post hoc* test).

(E) Diagram showing experimental timeline, and diagram of virus injection in the DR of SERT::Cre mice as well as VTA microinjection of ondansetron, ketanserin, or CNQX, and VTA optical stimulation of DR SERT terminals.

(F) VTA optical induced real-time or conditioning place preference was blocked by intra-VTA injection of ondansetron or CNQX, but not by ketanserin. All treatment groups were compared with ACSF group (ondansetron versus ACSF, chamber × group interaction: $F_{2, 24} = 4.187$, p = 0.028; CNQX versus ACSF, chamber × group interaction: $F_{2, 26} = 5.124$, p = 0.013; ketanserin versus ACSF, chamber × group interaction: $F_{2, 26} = 1.48$, p = 0.246, three-way ANOVA). Relative time spent in each chamber is represented as means ± SEM. Mice received a single intra-VTA microinjection of ACSF (n = 7), ondansetron (n = 7), ketanserin (n = 8) or CNQX (n = 8) 10 min before laser training. Intra-VTA ACSF injected mice showed preference to the laser-associated chamber on training day and test day in comparison with non-laser-associated chamber (*p = 0.0009, #p = 0.0008, Newman–Keuls *post hoc* test).

Scale bars: 10 μm in (A) and (B’); 40 μm in (B).

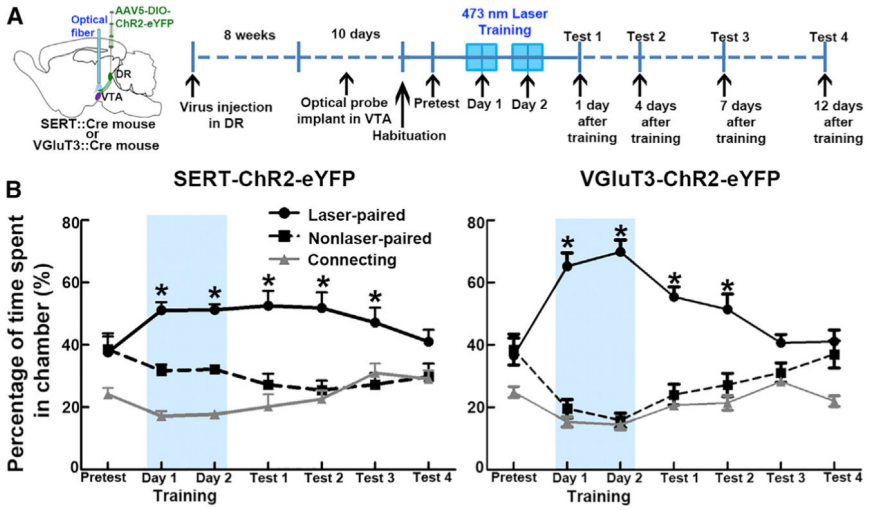

Figure 6. Comparison between the Conditioned Place Preference Induced by the Activation of VTA SERT-Fibers and the CPP Induced by the Activation of VTA-VGluT3 Fibers

(A) Diagram showing virus injection into the DR of SERT::Cre or VGluT3::Cre mice, VTA optical stimulation of DR-SERT-fibers or DR-VGluT3-fibers, and experiment timeline.

(B) On training days, both SERT-ChR2-eYFP and VGluT3-ChR2-eYFP mice spent more time in the chamber associated with the VTA optical stimulation. In tests 1 and 2, both SERT-ChR2-eYFP and VGluT3-ChR2-eYFP mice spent more time in the chamber in which optical stimulation was previously given. In test 3, SERT-ChR2-eYFP, but notVGluT3-ChR2-eYFP, mice spent more time in the chamber in which optical stimulation was given on previous training days. Relative time spent in each chamber is represented as means ± SEM (n = 10 each group). Blue rectangles indicate optical stimulation available in the laser-paired chamber on training days 1 and 2. Both SERT-ChR2-eYFP and VGluT3-ChR2-eYFP mice showed preference for the laser-associated chamber on training days and tests 1 and 2 in comparison with non-laser-associated chamber(group × day × chamber interaction: $F_{12, 216} = 4.342$, $p = 0.000001$, three-way ANOVA; *$p < 0.0001$ (see p value for each test in Table S2), Newman-Keuls *post hoc* test), but only SERT-ChR2-eYFP mice showed preference for laser-associated chamber in test 3 in comparison with non-laser-associated chamber (*$p = 0.00099$, Newman-Keuls *post hoc* test).

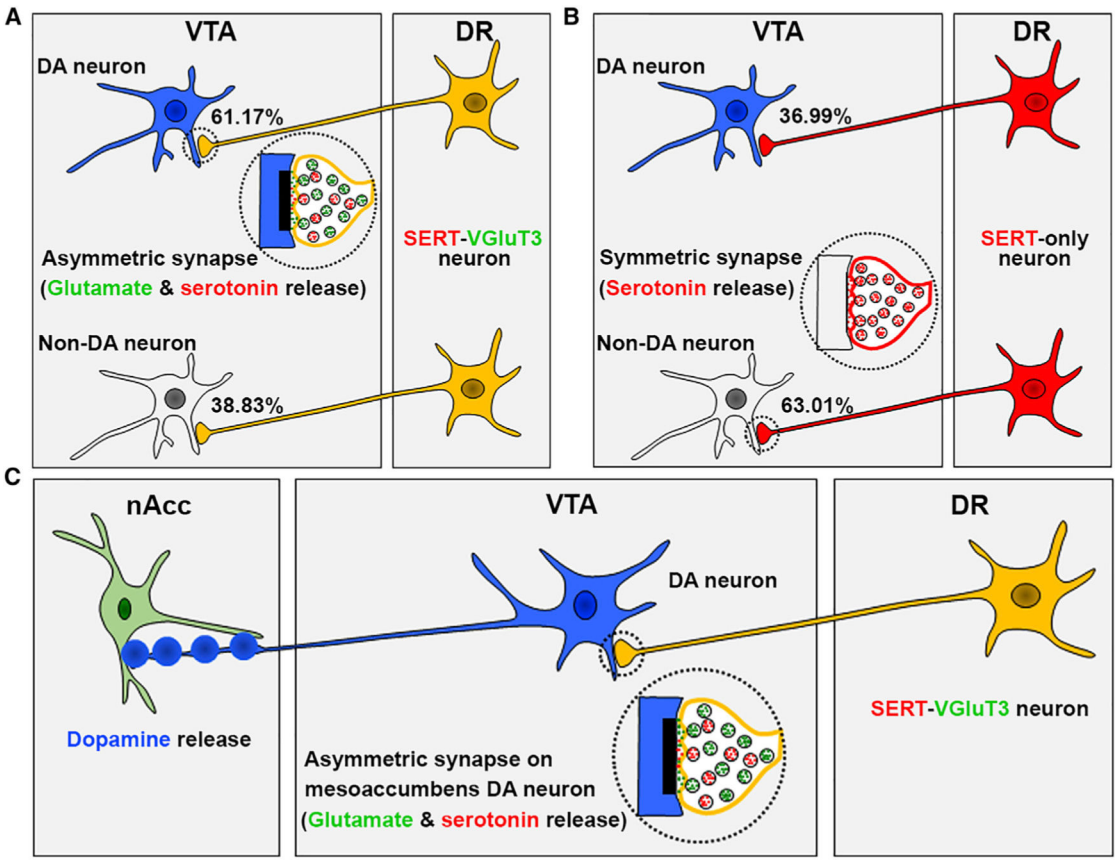

Figure 7. VTA Synaptic Connectivity by DR Serotonin Neurons

(A) DR dual-SERT-VGluT3 neurons establish asymmetric synapses mostly on dopamine neurons (61.17%) and less frequently on nondopamine neurons (38.83%).

(B) DR SERT-only neurons establish symmetric synapses mostly on nondopamine neurons (63.01%) and less frequently on dopamine neurons (36.99%).

(C) VTA mesoaccumbens dopamine neurons establish asymmetric synapses with a subset DR SERT-VGluT3 axon terminals, in which, the release of serotonin and glutamate evokes both dopamine release in the nAcc and reward.

KEY RESOURCES TABLE

REAGENT or RESOURCE	SOURCE	IDENTIFIER
Antibodies		
Mouse anti-tryptophan hydroxylase antibody	Sigma-Aldrich	CAT# T0678; RRID: AB_261587
Guinea pig anti-VGluT3 antibody	Synaptic System	CAT# 135204; RRID: AB_2619825
Rabbit anti-SERT antibody	Frontier Institute Co. Ltd	CAT# HTT-Rb-Af560–1; RRID: AB_2571775
Mouse anti-synaptophysin antibody	MilliporeSigma	CAT# MAB368; RRID: AB_94947
Mouse anti-TH antibody	MilliporeSigma	CAT# MAB318; RRID: AB_2201528
Goat anti-GFP antibody	Frontier Institute Co. Ltd	CAT# GFP-Go-Af1480; RRID: AB_2571574
Rabbit anti-FG antibody	MilliporeSigma	CAT# AB153; RRID: AB_90738
Alexa Fluor 594-affiniPure donkey anti-mouse	Jackson Immunoresearch Laboratories	CAT# 715–585-151; RRID: AB_2340855
Alexa Fluor 488-AffiniPure donkey anti-guinea pic	Jackson Immunoresearch Laboratories	CAT# 706–545-148; RRID: AB_2340472
Alexa Fluor 594-AffiniPure donkey anti-rabbit	Jackson Immunoresearch Laboratories	CAT# 711–585-152; RRID: AB_2340621
Alexa Fluor 647-AffiniPure donkey anti-mouse	Jackson Immunoresearch Laboratories	CAT# 715–605-151; RRID: AB_2340863
Dylight 405-AffiniPure donkey anti-mouse	Jackson Immunoresearch Laboratories	CAT# 715–475-150; RRID: AB_2340839
Alexa Fluor 488-AffiniPure donkey anti-goat	Jackson Immunoresearch Laboratories	CAT# 705–545-147; RRID: AB_2336933
Alexa Fluor 647-AffiniPure donkey anti-guinea pig (706–605-148	Jackson Immunoresearch Laboratories	CAT# 706–605-148; RRID: AB_2340476
Mouse anti-mCherry	Takara (Clontech)	CAT# 632543; RRID: AB_2307319
Rabbit anti-TH antibody	MilliporeSigma	CAT# AB152; RRID: AB_390204
Biotinylated goat anti-rabbit antibody	Vector Labs	CAT# PK-4001; RRID: AB_2336810
Biotinylated goat anti-mouse antibody	Vector Labs	CAT# PK-4002; RRID: AB_2336811
VECTASTAIN ABC-peroxidase Kit	Vector Labs	CAT# PK-4000; RRID: AB_2336818
Anti-mouse IgG coupled to 1.4 nm gold	Nanoprobes Inc.	CAT# 2001; RRID: not available
Anti-guinea pig IgG Fab' fragment coupled to 1.4 nm gold	Nanoprobes Inc.	CAT# 2055; RRID: not available
Anti-rabbit IgG coupled to 1.4 nm gold	Nanoprobes Inc.	CAT# 2003; RRID: not available
Cy5 Streptavidin	Jackson Immunoresearch Laboratories	CAT# 016–170-084; RRID: AB_2337245
Chemicals, Peptides, and Recombinant Proteins		
Cholera toxin B subunit (CTb) conjugated with Alexa Fluor® 594	Life technologies	CAT# C34777
Fluoro-Gold (FG)	Fluorochrome, LLC	CAT# Patent No. 4,716,905
Ondansetron	Sigma Aldrich	CAT# O3639
CNQX disodium salt hydrate	Sigma Aldrich	CAT# C239
Eticlopride hydrochloride	Tocris a Biotechne Brand	CAT# No1847
Fluoxetine hydrochloride	Tocris a Biotechne Brand	CAT# No 0927
Ketanserin (+)-tartrate salt	Sigma Aldrich	CAT# S006
Y-25130 hydrochloride	Tocris a Biotechne Brand	CAT# No 0380
Durcupan ACM epoxy resin	Electron Microscopy Sciences	CAT# 14040
Nanoprobe Silver Kit	Nanoprobes Inc.	CAT# 2012

REAGENT or RESOURCE	SOURCE	IDENTIFIER
Experimental Models: Organisms/strains		
Mouse: C57BL/6J	The Jackson Laboratory	CAT# 5657312; MGI:5657312
Serotonin transporter (SERT)::Cre mice	Mutant Mouse Regional Resource Centers	RRID: MMRRC:017260-UCD
Software and Algorithms		
GraphPad Prism 5.0	GraphPad Software, Inc	RRID: SCR_002798
Adobe Photoshop	Adobe Systems Incorporated	RRID: SCR_014199
ANY-maze video tracking system	Stoelting Co.	RRID: SCR_014289
Imaris microscopy software	Bitplane, Inc.	RRID: SCR_007370
Statistica 9	StatSoft, Inc.	RRID: SCR_014213